SWING UP AND STABILIZATION OF ROTARY INVERTED PENDULUM BY USING ON-OFF TYPE OF COLD GAS THRUSTER ACTUATORS

A THESIS SUBMITTED TO
THE GRADUATE SCHOOL OF NATURAL AND APPLIED SCIENCES
OF
MIDDLE EAST TECHNICAL UNIVERSITY

BY

YUSUF SİLİK

IN PARTIAL FULFILLMENT OF THE REQUIREMENTS
FOR
THE DEGREE OF MASTER OF SCIENCE
IN
MECHANICAL ENGINEERING

SEPTEMBER 2019

Approval of the thesis:

SWING UP AND STABILIZATION OF ROTARY INVERTED PENDULUM BY USING ON-OFF TYPE OF COLD GAS THRUSTER ACTUATORS

submitted by **YUSUF SİLİK** in partial fulfillment of the requirements for the degree of **Master of Science in Mechanical Engineering Department, Middle East Technical University** by,

Prof. Dr. Halil Kalıpçılar _____
Dean, Graduate School of **Natural and Applied Sciences**

Prof. Dr. M. A. Sahir Arıkan _____
Head of Department, **Mechanical Engineering**

Assist. Prof. Dr. Ulaş Yaman _____
Supervisor, **Mechanical Engineering, METU**

Examining Committee Members:

Assoc. Prof. Dr. Melik Dölen
Mechanical Engineering, METU _____

Assist. Prof. Dr. Ulaş Yaman
Mechanical Engineering, METU _____

Prof. Dr. Mustafa Kemal Özgören
Mechanical Engineering, METU _____

Assist. Prof. Dr. Ali Emre Turgut
Mechanical Engineering, METU _____

Assist. Prof. Dr. Masoud Latifi Navid
Mechatronics Engineering, THK University _____

Date: 06.09.2019

I hereby declare that all information in this document has been obtained and presented in accordance with academic rules and ethical conduct. I also declare that, as required by these rules and conduct, I have fully cited and referenced all material and results that are not original to this work.

Name, Last Name: Yusuf SİLİK

Signature :

ABSTRACT

SWING UP AND STABILIZATION OF ROTARY INVERTED PENDULUM BY USING ON-OFF TYPE OF COLD GAS THRUSTER ACTUATORS

SİLİK, Yusuf
M.S., Department of Mechanical Engineering
Supervisor : Assist. Prof. Dr. Ulaş Yaman

September 2019, 92 pages

In this study, swing up and stabilization of on/off type of cold gas thruster driven inverted pendulum is accomplished. First, pulse width modulator (PWM) design method is generated to obtain quasi-linear thrust output from on/off type of thruster. Than, single axis angle controller is designed. Designed angle controller and PWM scheme are tested and verified on single axis angle control test setup. Finally, an other freedom is attached to single axis test setup and rotary inverted pendulum (Furuta Pendulum) is obtained. By this way inherently unstable, under-actuated and on/off driven system is obtained. For swing up motion, energy method is applied. Balancing of the pendulum is achieved by observer based state feedback controller under small angle assumption and quasi-linear output from PWM driven thrusters.

Keywords: Rotary Inverted Pendulum, Furuta Pendulum, Cold Gas Thruster, Pulse Width Modulation

ÖZ

AÇ-KAPA TİP SOĞUK GAZ İTKİ SİSTEMİ EYLEYİCİLİ DÖNEL TERS SARKACIN KALDIRILMASI VE STABİLİZASYONU

SİLİK, Yusuf

Yüksek Lisans, Makina Mühendisliği Bölümü

Tez Yöneticisi : Dr. Öğr. Üyesi Ulaş Yaman

Eylül 2019 , 92 sayfa

Bu çalışmada aç/kapa soğuk gaz itki sistemi eylecili ters sarkacın kaldırma ve stabilizasyon kontrolü uygulandı. Öncelikle, aç/kapa çalışan soğuk gaz itki sisteminden doğrusal kontrol etkinliği alınabilmesi için darbe genişlik modülasyonu tasarımı yapıldı. Daha sonra tek eksen açısal pozisyon kontrolcüsü tasarlandı. Tasarlanan açısal pozisyon kontrolcüsü ve darbe genişlik modülatörü tek eksenli test sisteminde sınandı. Son olarak, tek eksenli test sistemine bir serbestlik derecesi daha eklenerek dönel ters sarkaç (Furuta Pendulum) test sistemi elde edildi. Sarkaç kaldırma hareketi için enerji tabanlı kontrol stratejisi uygulandı. Stabilizasyon kontrolcüsü için ise, küçük açı ve modüle edilmiş doğrusal kontrol etkinliği varsayımı yapılarak, gözleyici tabanlı durum geri besleme doğrusal kontrolcüsü kullanıldı.

Anahtar Kelimeler: Dönel Ters Sarkaç, Furuta Sarkacı, Soğuk Gaz İtki Sitemi, Darbe Genişlik Modülasyonu

To My Family...

ACKNOWLEDGMENTS

I would like to thank my supervisor Assist. Prof. Dr. Ulaş Yaman for his generous support, guidance and encouragements throughout my studies.

I wish my deepest gratitude to my family for their endless support throughout this study and my life. I sincerely thanks to my fiance for her understanding, patience and support during this study.

I also thank to my colleagues in Control Technologies Department of Roketsan Missile Inc. for their advises and supports during this work.

TABLE OF CONTENTS

LIST OF TABLES

TABLES

LIST OF FIGURES

FIGURES

LIST OF SYMBOLS AND ABBREVIATIONS

SYMBOLS

L	Length of base curve
F	Thrust force
ρ	Flow density
V	Flow velocity
s	Seconds
N	Newton
R	Resistence
L	Inductance
V	Voltage
i	Current
λ	Magnetic flux
x	Solenoid plunger position
δ	Total displacement of the plunger
N	Number of coil
W	Electric Power
A_e	Effective cross sectional area of flux path
μ_0	Permeability of air
k	Spring constant
b	Viscous coefficient
m	Solenoid plunger mass
P_u	Inlet pressure
P_d	Discharge pressure
d	Valve diameter
w	Mass flow rate

C_d	Flow coefficient of he valve
k	Specific heat ratio
Rg	Ideal Gas Constant
T_u	Inlet Temperature
Q	Volumetric flow rate
Hz	Hertz
T_{PWM}	Pulse width modulation period
T_{open}	Valve opening time interval
DC	Duty Cycle
T_{close}	Valve closing time interval
f_{PWM}	Pulse width modulation frequency
DV	Duty value
α	Rod angular position
J_{rod}	Moment of inertia of the rod
r_{rod}	Rod radius
θ	Angular position of the pendulum
L	Pendulum length
J_{A0}	Moment of inertia of the pendulum
m_{rod}	Mass of the rod
m_{pen}	Mass of the pendulum
g	Gravitational acceleration
E	Total energy of the pendulum
w_n	Natural Frequency
w_b	Bandwidth Frequency
ζ	Damping Ratio

ABBREVIATIONS

PWM	Pulse Width Modulation
PW	Pulse Width
RIP	Rotary Inverted Pendulum
RMP	Reaction Mass Pendulum
LED	Light Emitting Diode
ZOH	Zero Order Hold

CHAPTER 1

INTRODUCTION

1.1 Motivation

Cold gas thusters have been used in space industry since 1960s. They are preferred for all range of orbits and inter-planetary missions [1]. Main reasons of their popularity are their cost effectiveness, environmental friendly characteristics and being highly reliable systems.

Due to their simple structures and use of propellants which produce no contamination, it is easier to construct laboratory level cold gas thruster test setups. In addition to that, other types of thruster systems also use similar pneumatic valves. Although there are differences in terms of dynamical characteristics between the cold gas types and other types of thruster systems, control strategies those applied on the cold gas thrusters can also be applied on any kind of thruster systems with some modifications.

Inverted pendulum system is a classical control problem application that is used for decades. The system, whether it is rotary type or cartesian type, has inherently unstable, under-actuated and non-linear dynamical characteristics. Due to these dynamical characteristics, many researchers employed their newly proposed control schemes on it.

In literature, there are different types of inverted pendulums using different type of actuators. The most classical one is an electric motor directly controlling the rod or the cart position. Hydraulic and pneumatic cylinder actuated pendulums are also used widely.

In addition to those, there are inverted pendulum systems controlled by reaction control systems. Many applications use reaction masses and control moment gyroscopes as an actuator for the inverted pendulum system. Reaction masses and control moment gyroscopes are widely used for spacecraft attitude control applications.

In this work, another type of reaction control system, cold gas thruster, is used as an actuator for the rotary inverted pendulum system. Cold gas thrusters have not been used as an actuator for the inverted pendulum systems before. The main difference and challenge when compared with other types of actuators is that the cold gas thruster system used in this work is an on/off type of actuator. Thus, this works extends the difficulties of inverted pendulum system by adding on/off characteristics on the actuator.

Cold gas thrusters are generally used for stabilization of spacecrafts. Fuel sloshing is a problem encountered in spacecraft applications. For some applications, sloshing of the fuel should also be in consideration during the motion of the spacecraft for both its effect on the spacecraft dynamics and chemically unstable characteristics of the used fuel. Fuel slosh can be modeled as the pendulum and angular position of the pendulum model should also be controlled during the motion of the spacecraft. Hence, with the addition of another state, system becomes under-actuated and it is highly similar to the system used in this work.

To summarize, the motivation of this work stands on two pillars. The first one is that inverted pendulums have not been actuated by on/off type of thrusters before in literature. The other one is that it has high similarities with thruster actuated spacecrafts having slosh dynamics.

1.2 Scope of the Thesis

In this thesis, the model of the thrust control valve is given. Differences between the model and the real valve are examined. Design of linear controller is proposed for the single axis control application and the stabilization of the rotary inverted pendulum. Pulse width modulator is designed to use linear control methods with on/off type of actuators. Design method for pulse width modulator considering valve dynamics is

presented.

1.3 Limitations of the Study

The study has some restrictions which can be improved in future works. The following context highlights some of these limitations.

- In this work, only valve is modeled as a cold gas thruster system component. To be able to observe dynamics of other components, other components may also be modeled.
- During modeling and tests, air is preferred as a propellant. Instead of air, widely used cold gas propellants like nitrogen or helium can be used.
- Three axis attitude test setup, which is closer to real spacecraft control problems, can be used.
- Control structure in this work is limited by linear state feedback controller. Other nonlinear control topologies may also be applied on the system.

1.4 Outline

Outline of the rest of the thesis is as below.

Chapter 2 gives background information about the relevant topics to this thesis. Brief information about reaction control systems are presented. Cold gas thrusters, thrust control methods, inverted pendulum types and control strategies for inverted pendulums are examined.

Chapter 3 is about on/off valve characterization. Detailed mathematical model of a solenoid valve is presented and the valve is also characterized experimentally. Differences between the model and the experiments are observed and the model is updated later on.

Chapter 4 is about design of the pulse width modulator. PWM design restrictions are discussed. According to the valve dynamics, PWM frequency selection is given. Modulated valve output results are presented.

Chapter 5 is about controller design for the single axis and the inverted pendulum setups. In this chapter, linear control methods are utilized for both of the test setups. Simulation performances of the controllers and the modulated thrusters are presented.

Chapter 6 gives the details of the experimental test setups. First, working principles and used components are explained. Then, the results of the experiments are discussed.

The thesis is concluded with some remarks and discussions on future studies with Chapter 7.

CHAPTER 2

BACKGROUND

2.1 Introduction

In this chapter, background information about this work is presented under two main topics. These are cold gas thrusters and inverted pendulums. In addition to that how these two topics might be interrelated is explained.

In the upcoming section, history, working principles, thruster classification and usage areas of cold gas thrusters are explained. Then, thrust control methods used in spacecraft industry are investigated.

In the inverted pendulum section, the role of inverted pendulum in control theory is explained. Then, dynamically similar problems with inverted pendulums are explained. Later, controller types and inverted pendulum configurations used in literature are investigated. Finally, sloshing dynamics of spacecrafts which are similar to the thrust actuated inverted pendulums are explained.

2.2 Cold Gas Thrusters

In aircraft and spacecraft applications (satellite, launcher, missile, etc.), there are some conditions where it is not appropriate to use aerodynamics fins as control surfaces. Those conditions can be explained using aerodynamics force equation:

$$F \; \alpha \; \rho V^2 \tag{2.1}$$

According to the above equation, aerodynamic force is proportional to the medium density and the relative velocity between the fin and the medium. As a result, performances of control actuation fins are not sufficient at high altitude atmosphere, out of atmosphere and low velocity applications. In addition to these conditions, high maneuverability is not possible with the fin actuator due to the separation limits of the fin.

When control actuation fins are not appropriate as a control actuation system, one of the reaction control systems must be used. There are different types of reaction control systems. These are reaction wheels, control moment gyroscopes, magnetorquers and thrusters. In this thesis, control of thrusters is evaluated.

Reaction wheels use 2nd Law of Newton. By controlling the angular momentum of the wheel via an electric motor, control torque can be generated as a result of conservation of angular momentum. Control moment gyroscopes use gyroscopic effect for the generation of control torque. By controlling the angle of constant speed of the wheel via a gimbal, control torque can be obtained.

Magnetorquers use magnetic field of the earth to generate the required control torque. In this system, current flows through a coil and magnetic dipole moment is created. Cross product of earth magnetic field and the coil dipole moment generates control torque.

Thrusters are the most popular reaction control systems and widely used in spacecraft applications more than 60 years. They use 3rd Law of Newton to generate the control force. From conservation of momentum, gas expelled from the spacecraft generates the force in the reverse direction of the expelled gas direction. Amplitude of the force is proportional to the gas velocity and the mass flow rate of the gas. This phenomenon can be used as the control actuation system on aircraft or spacecraft applications.

Thrusters can be classified as cold, warm and hot gas thrusters. This classification is based on the output temperature of the expelled gases and given in Table 2.1. Warm and hot gas thrusters can be classified as mono-propellant and bi-propellant thrusters in terms of used number of propellants.

The main focus will be on the valve control; effects of the other components will

Table 2.1: Thruster Classification

Thruster Class	Temperature (Kelvin)	Specific Impulse (s)	Thrust (N)
Cold Gas	200-300	60-250	0.01-50
Warm Gas	500-1600	130-280	0.5-500
Hot Gas	Over 2600	300-450	1-4000

not be considered. On the other hand, by applying control strategies on the cold gas thruster, information about general thrust control will be obtained since similar flow control valves are used for different types of thrusters.

2.3 Thrust Control Methods

There are two different flow control valves to control the thrust of the actuation systems. These are continuously acting servo/proportional valves and the on/off acting valves. Servo/proportional valves have the advantage of controlling the thrust amplitude continuously. However, their disadvantages are having complex structures and high costs. In addition to these, servo/proportional valves are highly sensitive against dirty environments. On the other hand, on/off valves have simpler structures, less moving elements and they are highly cheap compared to the servo/proportional valves. The drawback of on/off valves is that they cannot control the flow continuously due to the nature of the valve and they have switching restrictions. Considering the aforementioned advantages, on/off valves are preferred for the thruster applications.

Common control techniques for on/off type of actuators are bang-bang control and pulse modulators. Bang-bang control requires nonlinear analysis. By using pulse modulators quasi-linear output can be obtained from on/off actuator and linear control techniques can be applied. This type of quasi-linearization results with very good approximation for the faster switching actuators. However, due to the switching restrictions, for the slower switching actuators, like solenoid valves, there will be big discrepancies between the desired and the actual outputs.

One of the most common pulse modulation technique is the pulse width modulation (PWM). PWM is a constant frequency averaging method that converts continues ref-

erence input signals to pulse signals. Many works presented in the literature related to the study are about PWM design for thrust control applications [2–8]. However, most of these works do not consider the switching restrictions of the valves and do not take into account the minimum and the maximum duty cycles of the valves for the designed pulse witdh (PW) modulators. Duty cycle limits are important control parameters for thruster applications. These parameters are directly related to the switching restrictions of the thruster valve. In literature, there are studies on this specific topic. Suzuki et al. [9] used pressure sensor to determine the minimum duty cycle of the PWM driven thruster valve. The work stated that the minimum duty cycle parameter is directly related to the dead-zone of the actuator. They made a PWM period adjustment trials to obtain the required performance. In our work, the relation between the duty cycle limits and the actuator dead-zone is used. However, the relationship between the duty cycle limits, PWM period and the valve characteristics are presented analytically and no trial and error process is required to obtain the desired performance. Jeon et al. [10] obtained opening and closing characteristics of the thrusters by performing experiments on thrust measurement. Experiment results were used to determine the limit cycle characteristics of the spacecraft setup. Bals and Kienitz [11] calculated the minimum and the maximum switching frequencies of their proposed modulation scheme by using valve opening and closing times. In present work, PWM frequency selection is done according to the required duty cycle limits.

PWM design for on/off valves and switching restrictions of on/off valves are studied on industrial applications in addition to the thruster applications. Taghizadeh et al. [12] modeled and identified a PWM driven on/off solenoid valve for servo-pneumatic applications. Relation between the solenoid current and the switching characteristics is used to identify the valve parameters. Topcu et al. [13] modeled and developed a PWM driven on/off solenoid valve for pneumatic actuators. They made current simulation and experiment to determine the switching characteristics of a solenoid valve. Switching characteristics were later used for PWM design. In this study, the relation between the solenoid current and the switching characteristics is also used to characterize the thruster valve.

2.3.1 Time Delay in Thrust Control Systems

For the cold gas thruster actuated systems, due to opening and closing time intervals of the thruster valve, a time delay occurs in the overall control system. While designing the controller, time delay should also be modeled to obtain required performance from the control system.

For a continuous time system, time delay can be modeled as below in Laplace domain where τ is the time delay [14]:

$$L\{u(t-\tau)\} = e^{-s\tau}U(s) \tag{2.2}$$

Although the modeling of a time delay is an easy task in Laplace domain, controller design is not possible with this model since the time time delay is modeled in non-polynomial form. To be able to overcome this problem, time delay can be approximated as below [14]:

$$\frac{1}{(1+\frac{s\tau}{n})^n} \tag{2.3}$$

For the given approximation, as n value increases better approximation is obtained.

In discrete time systems, time delay can be implemented on the system as z^{-n} where n is the number of integer sampling period in the delay time [15]. Thus, n can be calculated as

$$n = \frac{\tau}{T} \tag{2.4}$$

Jasper [16] modeled the thruster as a sign function with a delay. Since the model is constructed in discrete domain and the delays related to the thruster dynamics is an integer multiple of the sampling period, thruster delay is easily taken into account while designing the controller.

However, for the cases where delay is not an integer multiple of the sampling period, the delay cannot be modeled as directly via z^{-n}. For these cases, Thiran [17] proposed an analytical solution for designing a filter that approximates fractional delay in polynomial form. Form of the Thiran fractional delay filter is given below [18]:

$$H(z) = \frac{a_N z^N + a_{N-1} z^{N-1} + ... + a_0}{a_0 z^N + a_1 z^{N-1} + ... + a_N} \tag{2.5}$$

where a_0 to a_N:

$$a_k = (-1)^k \binom{N}{k} \prod_{i=0}^{N} \frac{D - N + i}{D - N + k + i} \tag{2.6}$$

$$a_0 = 1 \tag{2.7}$$

$$D = \frac{\tau}{T} \tag{2.8}$$

$$N = ceil(D) \tag{2.9}$$

2.4 Inverted Pendulum Control

Inverted pendulum system is an inherently unstable, nonlinear, non-minimum phase and under-actuated control problem that is widely used for decades as an experimental test setup to demonstrate and verify different kinds of control schemes. Swing-up, balancing, switching and trajectory control are the main tasks for the inverted pendulum test setups.

Inverted pendulum problem can be considered as an example for thrust vectoring during vertical launch, vertical take off and landing (VTOL) of aircraft, control of a robotic arm and humanoid robots.

Matsumoto [19] used the analogy of inverted pendulum problem for hovering strategy of VTOL unmanned aerial vehicles (UAV). Inverted pendulum analogy was also used for vertical launch of missiles [20, 21].

Inverted pendulum phenomena is also utilized commonly to stabilize unstable fuel slosh of spacecraft with sloshable fuel. Traditional way of minimizing the fuel slosh is to add baffles to the fuel tank. However, this method increases the weight of the spacecraft and adds structural complexity to it [22]. There are many works in the literature which use fuel slosh sensor and controller to overcome the slosh problem of spacecrafts [23–27]. By this way, the necessity of baffles disappears. Slosh dynamics are generally modeled as a pendulum or a mass-spring-damper system. Schematic of the simplified slosh dynamics as a pendulum given in Figure 2.1 [26]. In this Figure,

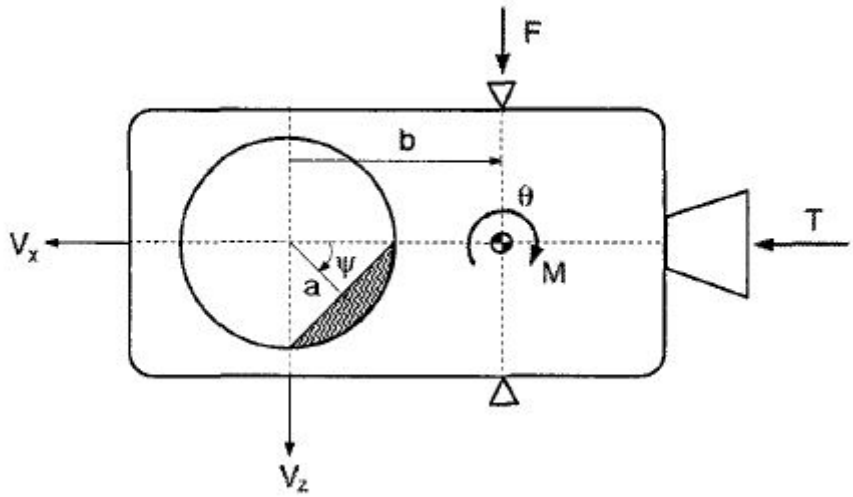

Figure 2.1: Schematic of Pendulum Slosh Dynamics [26]

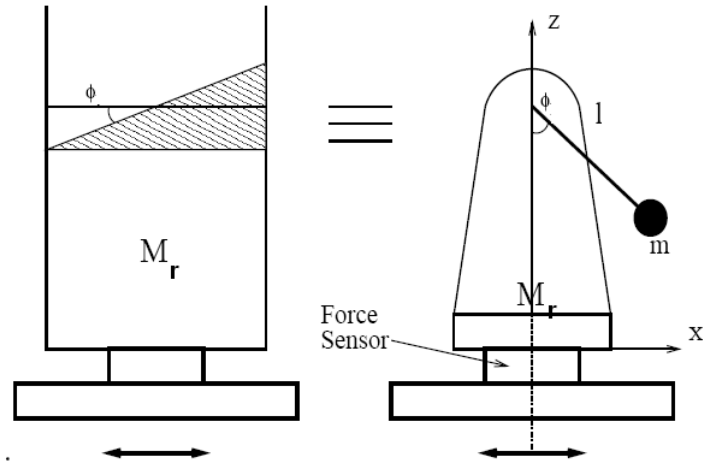

Figure 2.2: Slosh Mass Pendulum Model [24]

angle ψ is the pendulum angle and the controller tries to stabilize the pendulum angle as well as the roll, pitch and yaw angles. When slosh dynamics are modeled as a pendulum, the problem becomes the same with the stabilization of an inverted pendulum and rod tracking. Slosh control problem is also under actuated and unstable.

Bandyopadhyay [24] modeled slosh dynamics as a pendulum problem considering automobile industry, packaging industry, liquid cargo and liquid fluid rocket. In that work, sliding-mode under-actuated controller has been designed and verified by the laboratory scale test setup. 2.2 shows the schematic of how slosh dynamics are modeled as a pendulum mass.

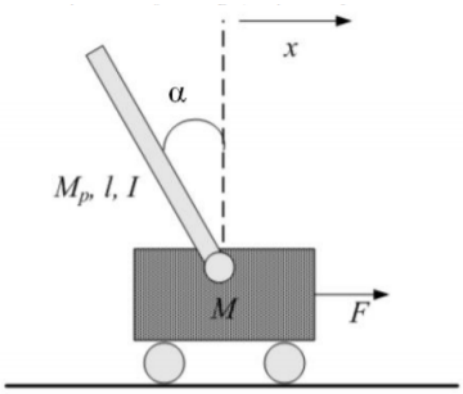

Figure 2.3: Schematic of a Cartesian Type of Inverted Pendulum [28]

There are mainly two types of inverted pendulums in terms of joint types. These are cartesian and rotary types. Main difference between them is the joint between the moving actuated mass and the ground. Regarding the rotary type, actuated mass is attached to the ground by a rovolute joint. For the cartesian type, moving mass is attached to the ground by a planar joint. Inverted pendulums can also be grouped by means of actuation. Mostly, moving mass is actuated by directly utilizing electric motors. In literature, other actuation types are pneumatic cylinders, hydraulic cylinders, reaction mass and control moment gyroscopes.

The most common type of inverted pendulum is the cartesian type. In this type, moving mass is actuated by a linear force and the pendulum is attached to the mass by a revolute joint. Schematic of a cartesian type of an inverted pendulum is given in Figure [28]. Different types of controllers are proposed for the control of cartesian type inverted pendulums. Kumar [28] proposed a linear quadratic regulator for balancing the motion. Chen [29] used sliding-mode control with fuzzy modeling for the same goal. Wai [30] proposed adaptive sliding-mode control for dual-axis cartesian inverted pendulum. El-Hawwary [31] proposed adaptive fuzzy control for the stabilization.

Rotary inverted pendulum test setup at first introduced by Furuta [32] in 1991. RIP is a system composed of rotating pendulum attached to a rotating arm by a revolute joint. Compared to the conventional pendulum on a cart system, RIP requires less space and less unmodeled dynamics since all of the joints are revolute joints. In addition to that, by using proper sensor wiring rotating arm can rotate infinitely. Infinite rotation

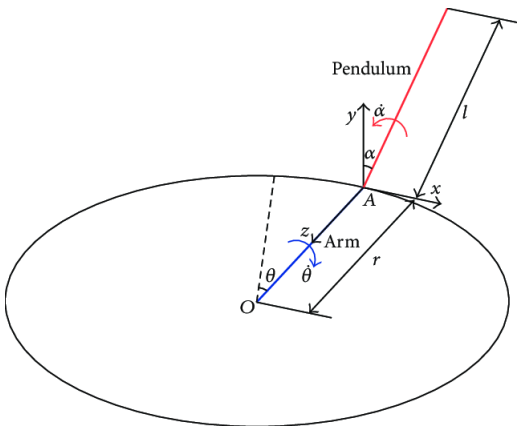

Figure 2.4: Schematic of a Rotary Inverted Pendulum [33]

provides convenience and large area for trajectory control during the experimentation. Schematic of a rotary inverted pendulum is given in Figure 2.4 [33].

Throughout the years, many different controller types are proposed and tested for rotary inverted pendulum test setups. Furata first [32] used a bang-bang type of state feedback algorithm for the swing up controller and optimal quadratic regulator for the balancing controller. Yang [34] proposed trajectory planning for swing up motion and adaptive neural network controller for the stabilization. Sainzaya [35] proposed and gave experimental results of Linear Quadratic Regulator with refined Proportional-Integral-Derivative controller for balancing the motion.

Another type of inverted pendulum is the reaction mass pendulum (RMP). It is a pendulum link attached to the ground by a revolute joint and rotating controllable mass is attached to the pendulum. Schematic of the reaction mass pendulum is given in Figure 2.5 [36]. Reaction mass control works according to the conservation of momentum and this phenomenon generally used for attitude control of spacecrafts. Andrievsky [22] uses energy based speed gradient control scheme for the swing-up motion and variable structural control for the stabilization of the RMP. Spong [37] experimentally compared feedback linearization and pole placement methods. The work resulted that feedback linearization and approximate linearization with pole placement method is comparable. Babiraju [38] gives linear and fuzzy methods for balancing of RMP.

There are experimental cartesian inverted pendulum setups driven by pneumatic or hydraulic cylinders [39–42]. Compared with the electrically driven ones, although

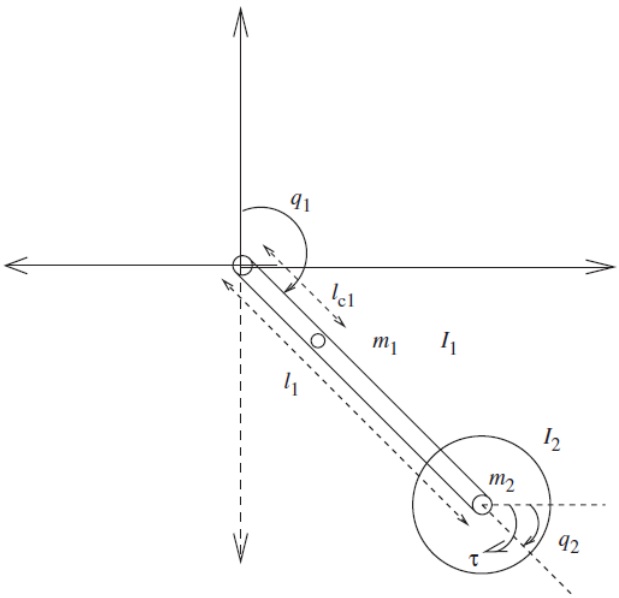

Figure 2.5: Schematic of Reaction Mass Pendulum [36]

similar control strategies can be applied, differences emerging from the pneumatic or hydraulic characteristics should also be considered and modeled for these types.

2.5 Research Opportunities

As explained in this chapter, inverted pendulums with various actuators are used as classical control problems throughout years. Generally, used actuators have servo characteristics and can provide required control actions. However, in this work, on/off type of cold gas thruster actuators are used for the inverted pendulum problem. In this work, previously untested inverted pendulum configuration is studied. In addition to that, performance of on/off actuator is examined for an unstable and under-actuated control system.

There is a similarity between the dynamics of inverted pendulum with on/off actuators and the dynamics of thruster actuated spacecraft with fuel slosh dynamics. Fuel slosh can be modeled as a pendulum attached to a spacecraft [24]. By assuming the center of mass position of the fuel is known, control strategies that obtained from this work can also be employed on the fuel slosh problem.

CHAPTER 3

ON/OFF VALVE CHARACTERIZATION

3.1 Introduction

In this work, PW modulated signal will be applied on the solenoid valve. Solenoid valves are widely used as industrial valves. They are also preferred for space and military applications. In a solenoid valve, there is a coil around a moving plunger. When current is applied, magnetic force is produced and the plunger moves. By this movement, the plunger opens or closes the valve depending on the valve configuration.

Two way normally closed valve will be used in this dissertation. To determine the control parameters of the PWM application, validity of the valve model is important. Opening and closing characteristics of the valve must be obtained precisely. Characteristics of the solenoid valve is obtained by modeling and experiments.

3.2 Characterization via Modeling

Solenoid valve can be modeled as four subsystems. These are electrical, magnetic, mechanical and pneumatic subsystem. These four subsystems will be modeled separately and their relations between them will be investigated.

3.2.1 Electrical Subsystem

The electrical subsystem of the solenoid valve can be modeled as serial connected resistance (R), inductance (L) and voltage (V) source. However, the inductance of the valve changes due to the movement of the solenoid plunger.

Elemantal equation that gives the voltage drop across resistance:

$$V_R = Ri \tag{3.1}$$

Elemantal equation that gives the voltage drop across inductance:

$$V_L = \frac{d\lambda(x)}{dt} \tag{3.2}$$

Regarding the above equation, flux linkage of magnetic actuator (λ(x)) is directly depends on the motion of the solenoid plunger. As a consequence, there occur changes on the flux linkage and on the inductance of the circuit. Equation of the flux linkage:

$$\lambda = L(x)i \tag{3.3}$$

Voltage drop across inductance in terms of inductance:

$$V_L = \frac{d\lambda(x)}{dt} \tag{3.4}$$

$$V_L = L(x)\frac{di}{dt} + i\frac{dL(x)}{dt} \tag{3.5}$$

Compatibility equation according to Kirchhoff's voltage law:

$$V + V_R + V_L = 0 \tag{3.6}$$

As mentioned before, inductance depends on the movement of the solenoid plunger. In literature, for modelling the inductance, there are different approaches according to the requirements of the system. These models are linear or high order nonlinear models. Makled [43] proposed 3rd order approximation using empirical approach:

$$L(x) = Ax^3 - Bx^2 + Cx + 0.16 \tag{3.7}$$

Since the solenoid plunger displacement is in the order of millimeter, change in the inductance is close to linear. If the open and closed values of inductance are know,; linear model can be used safely in the model.

$$L(x) = L_{off} + \frac{L_{off} - L_{on}}{\delta}x \tag{3.8}$$

3.2.2 Magnetic Subsystem

Magnetic subsystem calculates the magnetic force on the solenoid plunger when voltage is applied on the solenoid. Magnetic force on the steel plunger is a function of the magnetic flux and the current on the coil of the solenoid.

Inductance of the coil is a function of the solenoid plunger as mentioned before:

$$L(x) = N^2 L_o f(x) \tag{3.9}$$

Equation of the magnetic flux[44]:

$$\lambda(i, x) = N^2 L_o i f(x) \tag{3.10}$$

Equation of magnetic force:

$$F = \frac{\delta W}{\delta x} \tag{3.11}$$

where:

$$W = \int \lambda di = \frac{N^2 L_o i^2}{2} f(x) \tag{3.12}$$

Thus, the magnetic force applied on the plunger becomes

$$F = \frac{N^2 L_o i^2}{2} \frac{df(x)}{dx} \tag{3.13}$$

L_o can be approximated as

$$L_o = \frac{A_e \mu_o}{2} \tag{3.14}$$

The position dependence is related with the change in the total air gap:

$$f(x) = \frac{1}{x_0 - x} \tag{3.15}$$

Then, the force applied on the solenoid plunger is determined as

$$F = \frac{N^2 A_e \mu_o i^2}{4} \frac{1}{(x_0 - x)^2} \tag{3.16}$$

3.2.3 Mechanical Subsystem

Mechanical subsystem of the solenoid valve can be modeled as mass, spring and damper system where the solenoid plunger is the moving mass. Forces acting on the plunger of the solenoid are spring force, viscous friction force, flow pressure force

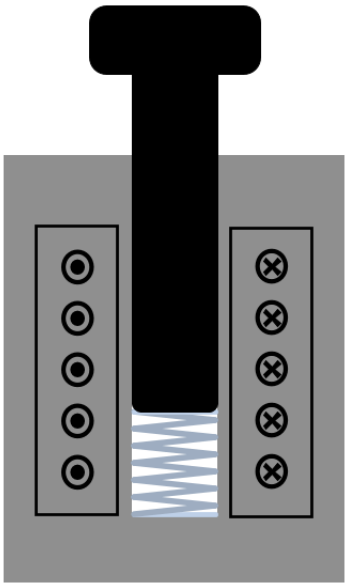

Figure 3.1: Mechanical Subsystem

and the magnetic force. In addition to these, preloaded spring force keeps the valve closed.

For normally closed solenoid valve configuration, magnetic and flow force tend to open the valve while other forces tend to close the valve. Schematic of the described mechanical subsystem is given in Figure 3.1.

Elemental spring force equation:

$$F_k = kx \tag{3.17}$$

Elemental viscous force equation:

$$F_b = b\dot{x} \tag{3.18}$$

Inertia force due to D'Alembert principle:

$$F_m = m\ddot{x} \tag{3.19}$$

Preloaded force is related with the spring constant and the preload distance. Valve manufacturer can supply these information or directly preloaded force. Pressure force equation:

$$F_{pre} = \frac{(P_u - P_d)\pi d^2}{4} \tag{3.20}$$

Pressure force is the function of the inlet and the discharge pressure. When the valve is opened, pressure changes due to the capacitive effect of the fluid. It is difficult to

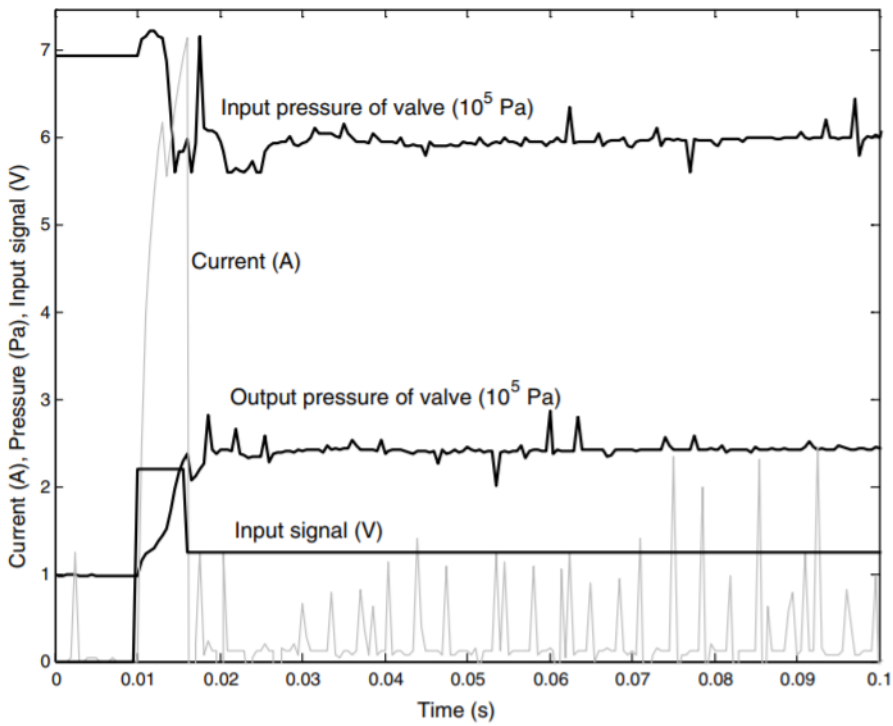

Figure 3.2: Pressure Force Experiment [45]

simulate this condition. Topcu [45] experimentally showed the inlet and the discharge pressure changes in Figure 3.2. In this work ,for simplicity, pressure changes will be omitted and pressures will be taken as constant.

Compatibility equation is

$$F_p + F_M - F_k - F_b - F_m - F_{pre} = 0 \tag{3.21}$$

3.2.4 Pneumatic Subsystem

In this subsystem, the mass flow rate of the valve is calculated first and then the thrust force. The main difficulty of pneumatic systems is the high compressibility of the working fluid. To obtain a reliable system, compressibility of gases must be added to the model. Compressible flow equations are derived from the fundamental thermodynamics and gas dynamics books [46]. These equations will be directly used in this model to obtain a pneumatic model. Below equation calculates the mass flow

rate.

$$\frac{w}{x} = C_d \sqrt{\frac{k}{Rg}\left(\frac{2}{k+1}\right)^{\frac{k-1}{k+1}}} \frac{P_u}{\sqrt{T_u}} f_1\left(\frac{P_d}{P_u}\right) d \tag{3.22}$$

where f_1 function:

$$f_1\left(\frac{P_d}{P_u}\right) = \begin{cases} \sqrt{\frac{2}{(k-1)\left(\frac{2}{k+1}\right)^{\frac{k+1}{k-1}}}} \left(\frac{P_d}{P_u}\right)^{\frac{1}{k}} \sqrt{1 - \frac{P_d}{P_u}^{\frac{k-1}{k}}}, & \text{for } \frac{P_d}{P_u} > 0.528 \text{ (For Air)} \\ 1, & \text{for } \frac{P_d}{P_u} < 0.528 \text{ (For Air)} \end{cases} \tag{3.23}$$

For our case, f_1 function is always equal to 1 and under the ideal gas assumption k and R values are constant. Then, a constant variable can be defined as

$$c_1 = C_d \sqrt{\frac{k}{Rg}\left(\frac{2}{k+1}\right)^{\frac{k-1}{k+1}}} \tag{3.24}$$

Thus, the mass flow rate equation becomes

$$\frac{w}{x} = c_1 \frac{P_u}{\sqrt{T_u}} \tag{3.25}$$

Thrust force is calculated using the outputs of the pneumatic model. From the conservation of momentum equation, force will be applied on the system. This equation is given below:

$$F = \rho Q V \tag{3.26}$$

Since the mass flow rate can be defined as below

$$w = \rho Q, \tag{3.27}$$

thrust force equation becomes

$$F = wV. \tag{3.28}$$

When the equation is examined, thrust force is proportional to the mass flow rate and the exit velocity. Without converging/diverging nozzle, flow will be chocked at the valve exit and the flow velocity is constant for every opening of the valve. However, change in the mass flow rate will affect the resulting thrust.

3.2.5 Subsystem Interactions

In this section, interactions between predefined subsystems are explained. Figure 3.3 gives relations between the four subsystems. Voltage is applied on the electrical

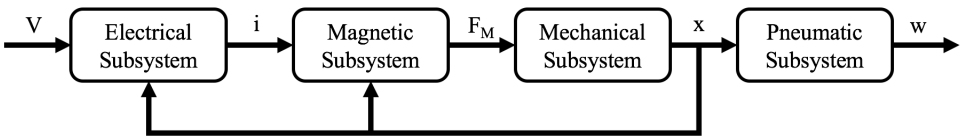

Figure 3.3: Solenoid Valve Subsystems

Table 3.1: Parameters of the Solenoid Valve Model

V	24 V	P_u	5 Bar
R	32 Ohm	P_d	1 Bar
L_{off}	0.14 H	d	8.6 mm
L_{on}	0.22 H	F_{pre}	200 N
δ	0.46 mm	C_d	0.65
N	2000	k	20000 N/m

subsystem and the current is the output of the subsystem. Magnetic subsystem takes current as an input and gives magnetic force as an output. Input of the mechanical subsystem is the magnetic force and the output is plunger position. Input of the pneumatic subsystem is plunger position and the output is mass flow rate. In addition to the electrical inputs, magnetic subsystem takes plunger position as an input since the inductance is dependent on the plunger position.

3.2.6 Solenoid Valve Model Results

In this section, results of the solenoid valve model are investigated. By this way, opening and closing characteristics of solenoid valve are obtained. In addition to that, relationship between valve opening-closing and solenoid current is investigated. Model parameters are given in Table 3.1.

Figure 3.4 shows the plunger position simulation when voltage is applied on the model and Figure 3.5 shows the current simulation when voltage applied on the model. As seen from current simulation figure, there occurs local maxima and minima sequence during the opening motion. This occurs due to the sudden inductance increase due to the movement of the solenoid plunger. This phenomenon is explained in electrical subsystem section. Local maxima point gives the motion starting instant of the solenoid plunger and the local minima point gives the motion stopping instant. When plunger position and current graphs are examined, plunger movement and lo-

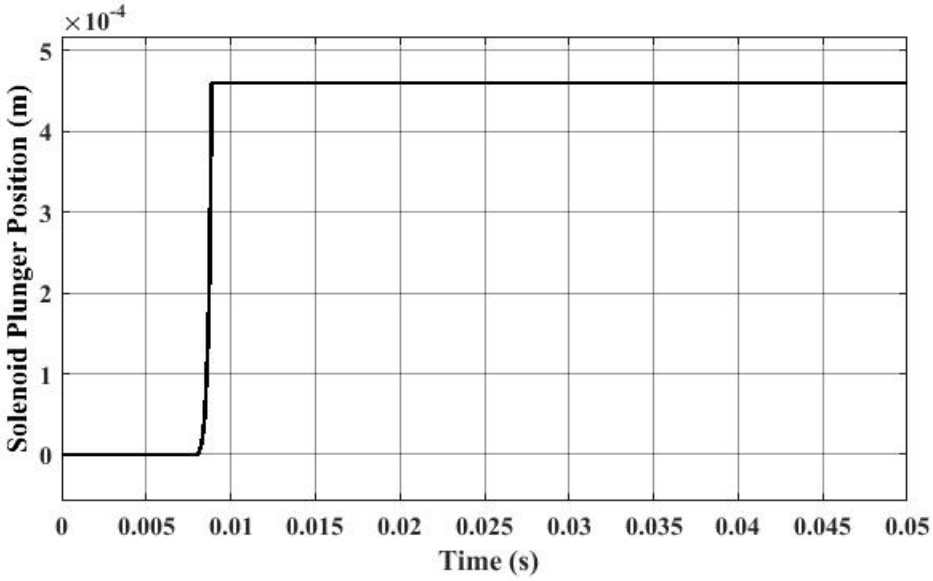

Figure 3.4: Valve Opening Plunger Position Simulation

cal maxima-minima occurrence instants exactly overlap. This is expected since the movement of the plunger changes the inductance other than the solenoid current. This phenomenon is important since during opening and closing motion current is measurable unlike the solenoid plunger motion. This characteristic is used in characterization via experiment section.

Figure 3.6 shows plunger position simulation when close command is applied (voltage is removed from electrical subsystem). Figure 3.7 shows the current simulation during the same valve closing motion. Similar to the opening case, this time local maxima and minima sequence occurs during the closing motion. This local maxima and minima sequence instants overlaps with the solenoid plunger closing motion. This is also expected since the inductance of the solenoid circuit increases when the solenoid is closed. Similar to the opening case, this characteristic is also used in characterization via experimentation section.

According to Figures 3.4 and 3.5 solenoid starts its motion 8 milliseconds after the voltage is applied and the total time of opening is 9 milliseconds. According to Figures 3.6 and 3.7 solenoid starts its motion 26 milliseconds after the voltage is removed and it completes its closing motion in 27 milliseconds. These solenoid opening and closing characteristics are used for PWM design. However, firstly, differences between the model and the experiment results will be investigated in the next section.

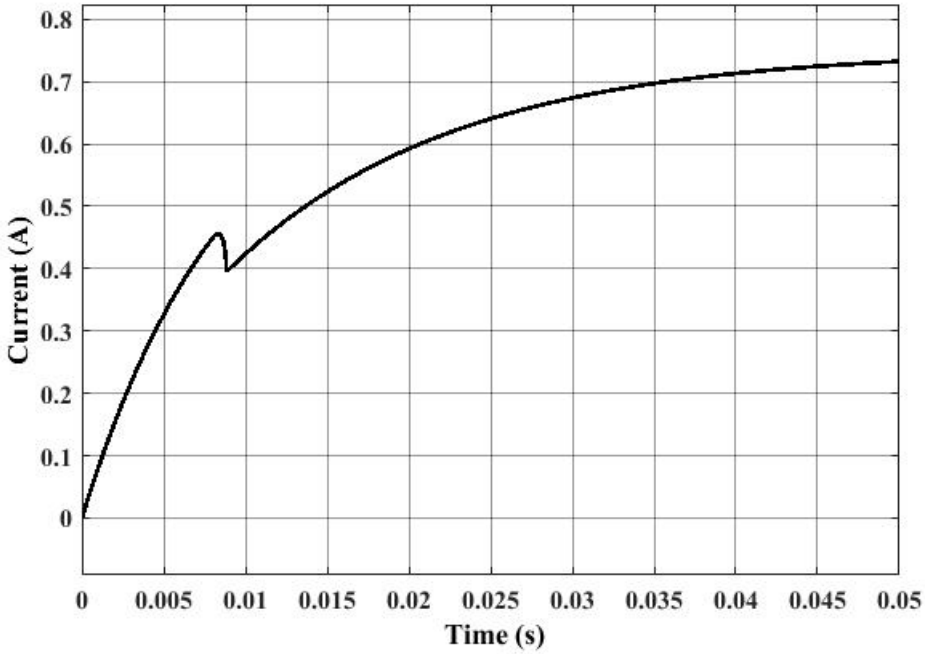

Figure 3.5: Valve Opening Current Simulation

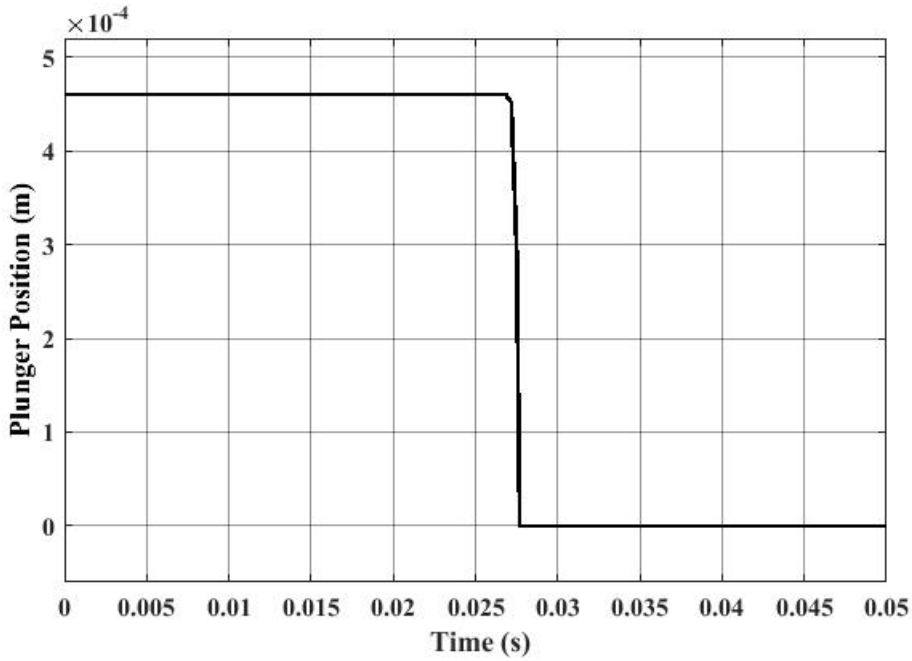

Figure 3.6: Valve Closing Plunger Position Simulation

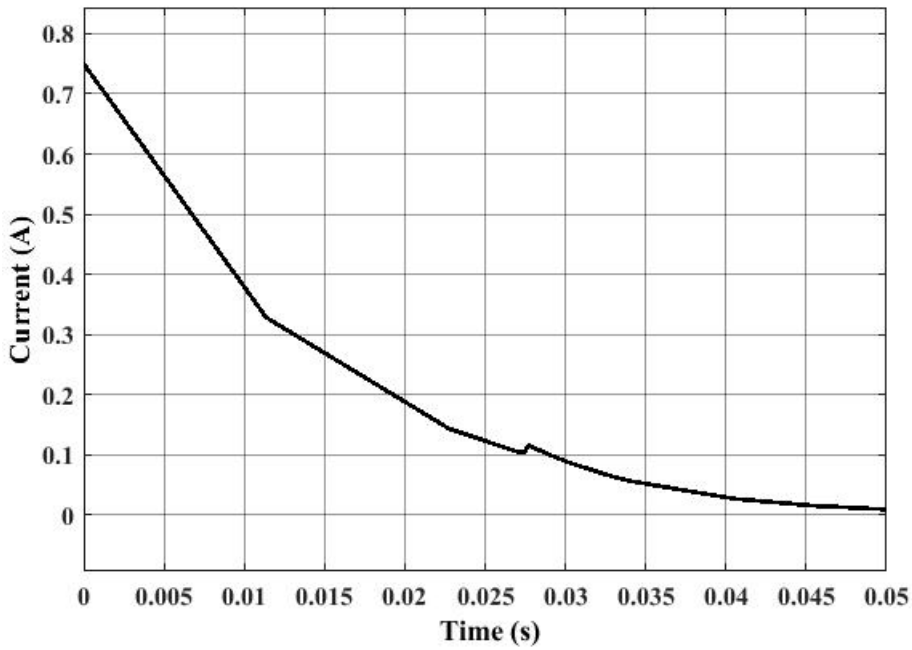

Figure 3.7: Valve Closing Current Simulation

3.3 Characterization via Experimentation

In this section, readily available solenoid valve will be characterized by experiments. As explained in the modeling section, there is a close relationship between the solenoid plunger motion and the solenoid current. Since the inductance of the solenoid circuit changes with the movement of the solenoid plunger, derivative of the current suddenly changes at the instant of the opening of the solenoid valve. Derivative of the solenoid current is given in Figure 3.8. As a consequence, there occurs local minima and maxima points during the valve opening and closing as given in Figures 3.5 and 3.7. Although measuring the movement of the solenoid plunger is hard to do, the solenoid current can be measured during opening and closing. These characteristics will be used to characterize the readily available valve.

Experiments are carried out using solenoid thruster valve, power supply, oscilloscope and real time target machine to obtaine the valve signal. For this experiment, it is advantageous to use the system that is close to the final system. Thus, the delays originated from voltage rising time and signal delays are also included in the characterization.

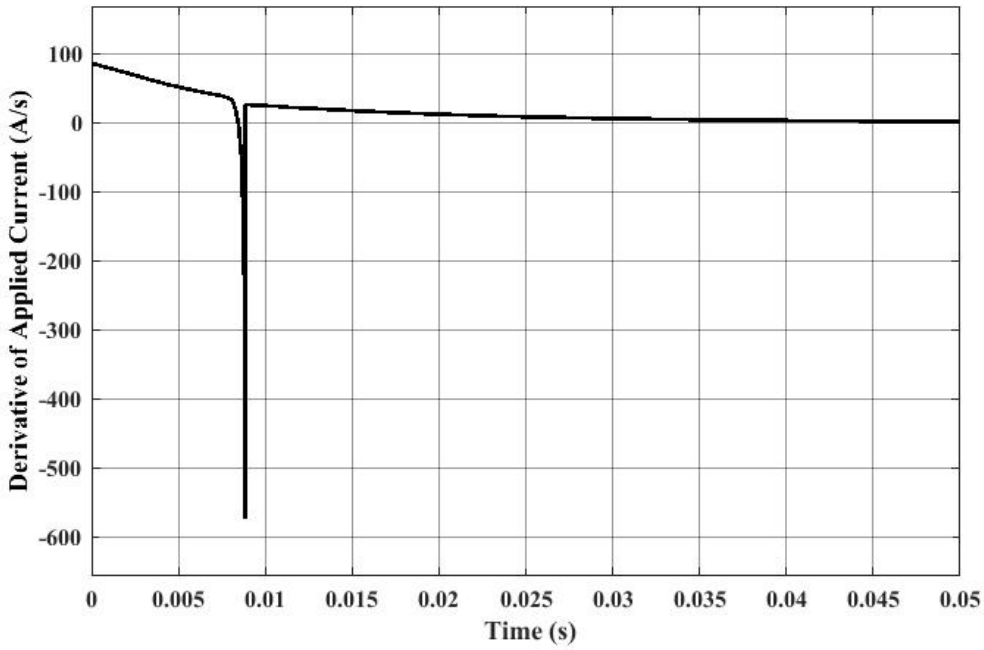

Figure 3.8: Derivative of Current During Valve Opening Simulation

Figure 3.9 shows the rising of the current during valve opening experimentation. According to the figure, the total opening time of the thruster valve is about 12 milliseconds.

Figure 3.10 shows the falling of the current during valve closing experimentation. According to the figure, the total closing time of the thruster valve is about 30 milliseconds.

3.4 Model Experiment Comparison and Model Update

In this section, the model and the experiment results are investigated. Discrepancies between the model and the experiment results are observed. Source of the discrepancies are investigated and finally the model is updated according to the results of the experiment.

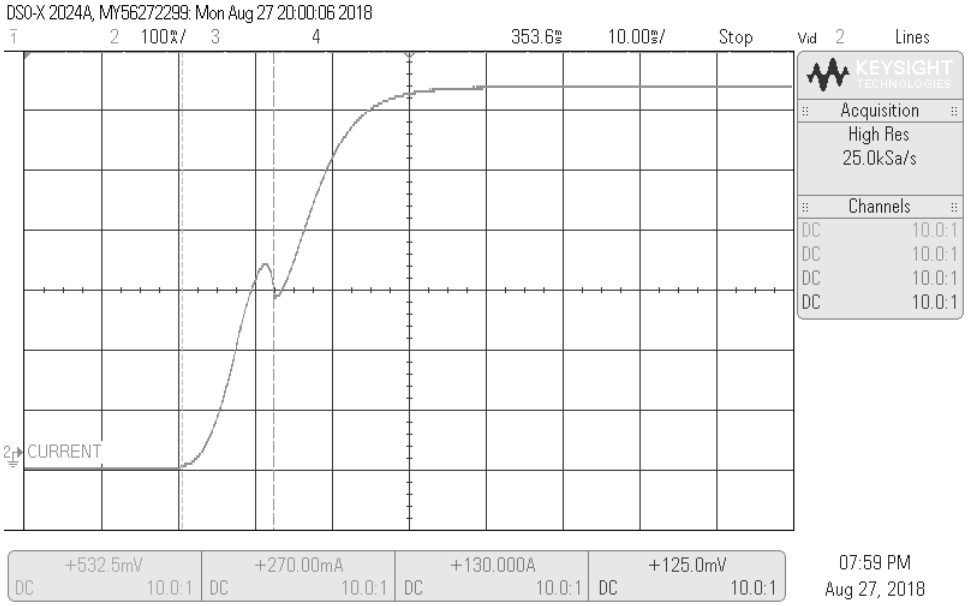

Figure 3.9: Valve Opening Current Experiment

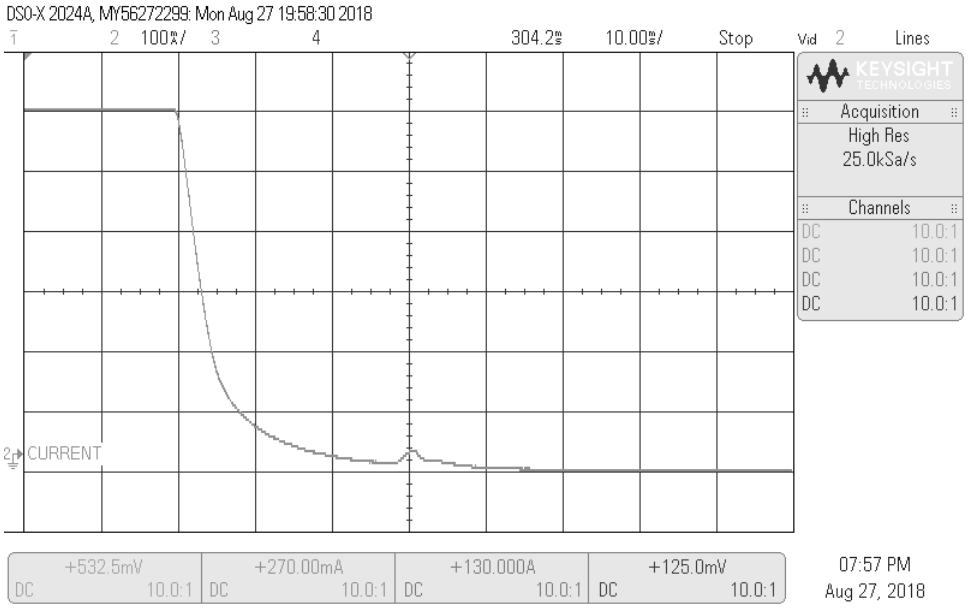

Figure 3.10: Valve Closing Currrent Experiment

3.4.1 Model Experiment Comparison

When compared, model and experiment results discrepancies are observed for opening and closing time interval of the solenoid valve. From the model, opening time of the solenoid is found as 9 milliseconds, However, it is found as 12 milliseconds experimentally. Solenoid closing time interval is found as 27 milliseconds, whereas it is found as 30 milliseconds in the experiment.

While modeling the solenoid valve, most of the required valve parameters are obtained from both valve manufacturer and measurements. During modeling, due to the lack off parameters (non-measurable and non-provided parameters), few assumptions are made on the model. Characteristic differences between the model and the experiment results are due to the results of miss-measurements of some parameters or made assumptions.

Another source of difference between the model and the experiment result is the input voltage rising time of the solenoid circuit. In model, the voltage is applied as a step input however for the real case it takes some time to settle the voltage to the desired value. Figure 3.11 shows voltage and current rise during the valve opening. As seen from the figure, voltage settling time takes more than 10 milliseconds. By considering the opening time interval magnitude, voltage rising time interval magnitude affects the valve characteristics.

Similar with the opening case, while modeling, the close command is also applied as a step command. As given in Figure 3.12, the time interval of voltage settling to zero also takes more than 10 milliseconds. By considering the closing time interval magnitude, voltage falling time interval magnitude affects the valve characteristics.

At the beginning of this section, it is stated that the experiment should be carried out close to the final version of the system. Advantage of this can be seen from the voltage rise and fall plots. Voltage delays related to the controller, voltage supply, cabling etc. are all included in the characterization.

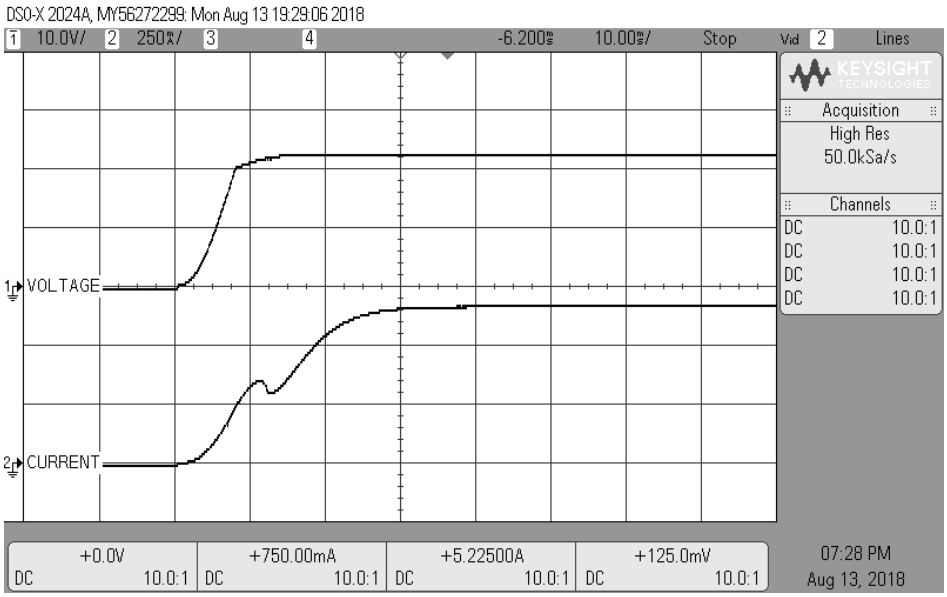

Figure 3.11: Voltage Measurement During Valve Opening

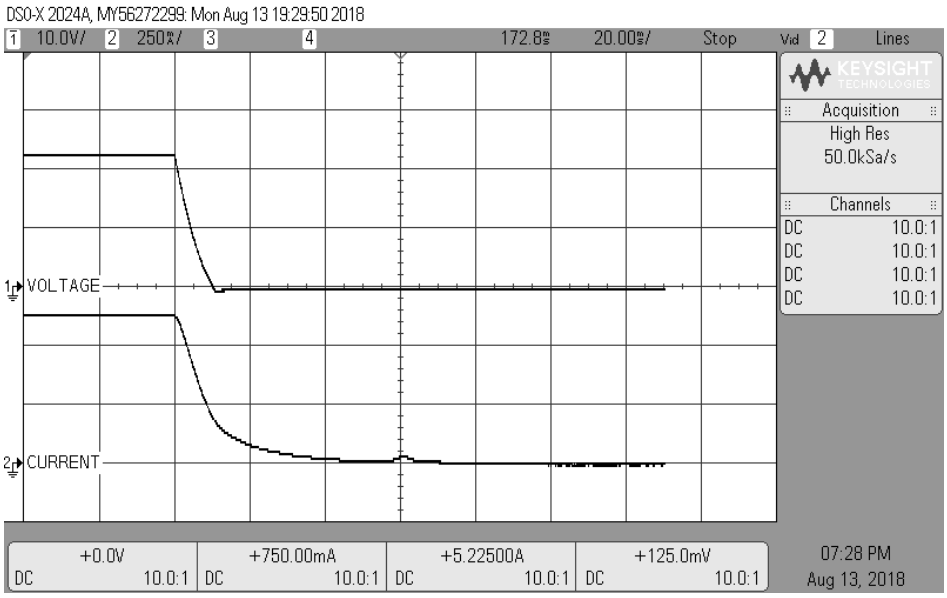

Figure 3.12: Voltage Measurement During Valve Closing

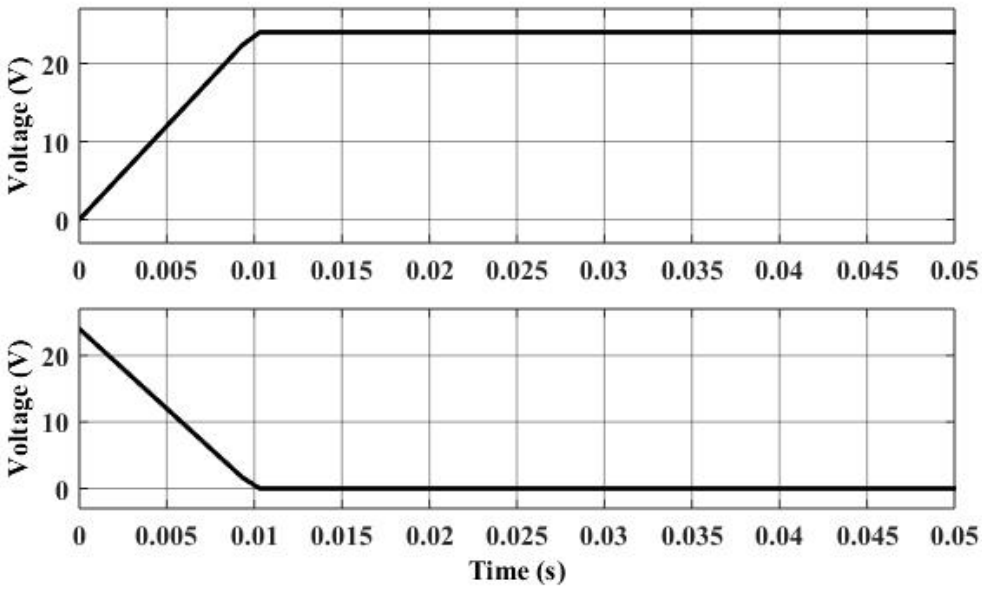

Figure 3.13: Modified Voltage Input

3.4.2 Model Update According to Experiment Result

In previous section, the discrepancies between the model and the experiment results are investigated. In this section, with the help of the experiment result, the model will be updated and a model close to the real system will be obtained. In previous section, the current experiment showed that it takes some time to settle the input voltage to the desired value. When Figures 3.11 and 3.12 are investigated, it is concluded that the input voltage increases and decreases close to linear ,respectively. As a result ,for the model, using ramp input instead of step input is closer to the real system. This is achieved using 100 V/s rate limiter at the inlet of the solenoid valve model. Output of the rate limiter for opening and closing cases are given in Figure 3.13. Figure 3.14 shows current simulation during the opening motion after the model is updated with the rate limiter. According to the figure, the opening time interval is approximately 12 milliseconds and it is the same with the experiment result. Similarly, Figure 3.15 shows current simulation during the closing motion after the model is updated with the rate limiter. According to the figure, closing time interval is approximately 31 milliseconds and highly close to the experiment result.

In this section, a model highly close to the experimental valve is achieved with the addition of the rate limiter. As a result, this model is used to verify the designed

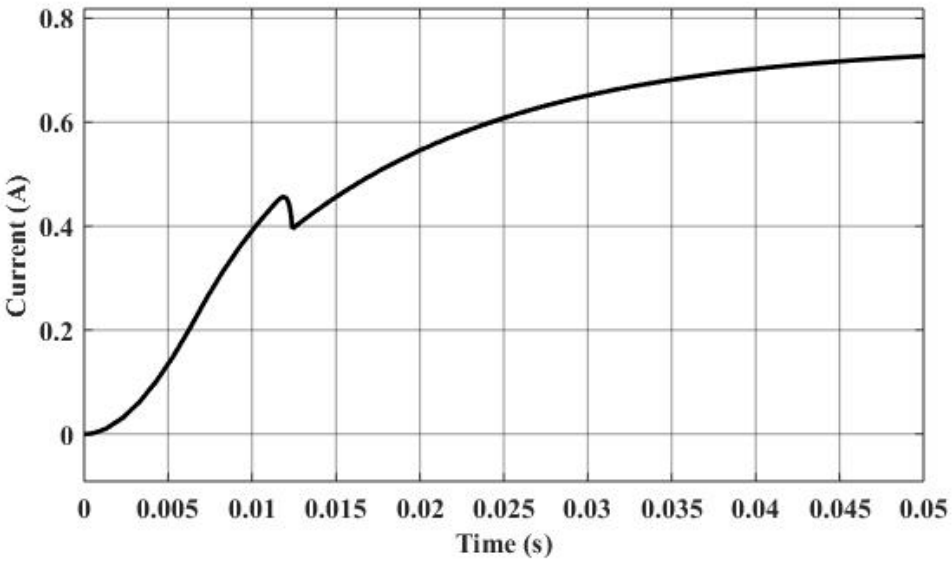

Figure 3.14: Updated Model Current During Opening Motion

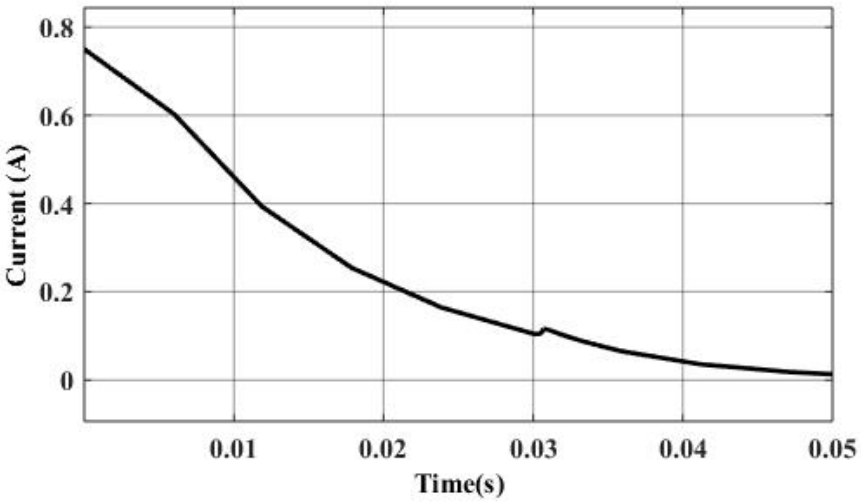

Figure 3.15: Updated Model Current During Closing Motion

modulator and the controller in the next sections.

3.5 Closure

In this chapter, the characteristics of an on/off (solenoid) valve are obtained. First, the mathematical model of a solenoid valve is constructed by using solenoid valve parameters. By using the model, opening and closing time intervals of the valve is found. Other than that, with the help of the constructed model, the relationship between the peaks of a solenoid current and the plunger movement instant is revealed.

Knowing that there is a relationship between the current peaks and the plunger movement instants, valve characteristics are also found by experimentation. Discrepancies are observed between the model and the experimentation. The main reason of the discrepancies is interpreted as a voltage rising behaviour during the experimentation. It is concluded that the input voltage has a rising slope for the real case and cannot be supplied as a step input. According to this conclusion the input voltage is rate limited in the model.

CHAPTER 4

PWM DESIGN METHOD

4.1 Introduction

In this chapter, PWM is designed according to the valve characteristics obtained in the previous chapter. PWM is a constant frequency modulation method widely used for digital control, hardware controllers and communication [47]. PWM constructs constant frequency with variable width pulse signals according to the input analog signal level. Figure 4.1 gives the relation between the input and 20 Hz PW modulated signals. PWM takes duty value as an input and converts the signal to the on and off commands. Output signal is on for a duration of duty value times the selected constant PWM period and it is off for the rest of the cycle.

Digital controllers are widely used due to their cost and weight effectiveness. PWM technique is applicable with digital controllers without using digital to analog converters. Since the physical systems generally behave as low pass filters using a greater frequency than the bandwidth frequency of the system, continuous response can be obtained. Thus, without the need of continuous signals, PWM is applicable on continuously acting devices and actuators such as LEDs and electric motors.

Another usage area of PWM method is on/off devices like solenoid valves. By applying PWM method on the on/off valves, they can be used as control valves, an alternative to servo-proportional valves. In this work, PWM is also applied on the on/off device.

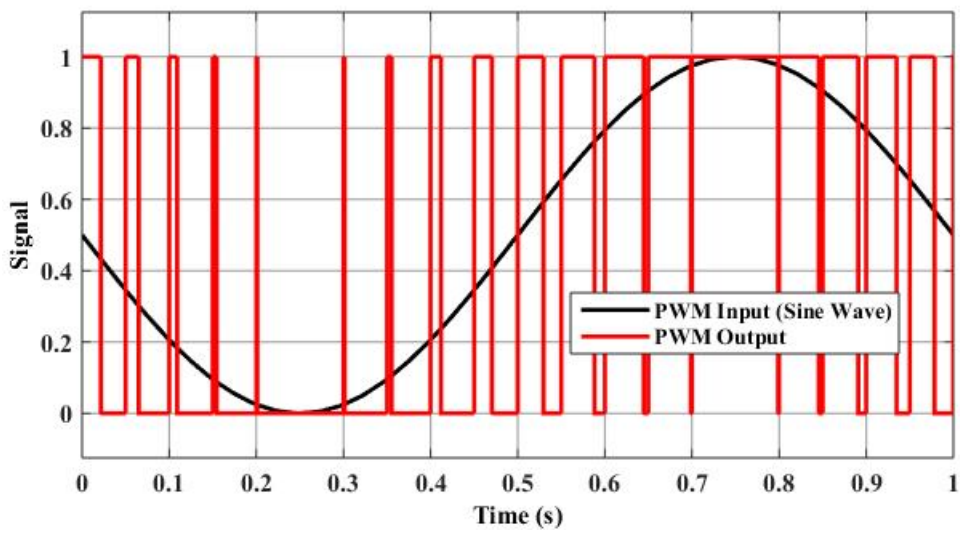

Figure 4.1: Illustration of PWM Working Principle

4.1.1 Restrictions of PWM Design

In this section, restrictions while designing PWM for a solenoid valve are explained. For this work, prepared solenoid valve model is used. To explain switching restriction several modulated inputs are applied on the model.

Reasons of switching restriction are the delays caused by the opening and the closing time intervals. Because of these delays, open or close commands must be applied in certain time intervals on the valve to obtain the desired output.

Figure 4.2 shows the model output for 10 Hz frequency 10 % duty value PW modulated input signal. According to the figure, the valve cannot be opened with the given signal. This can also be seen by the current output since there is no minima or maxima occurrence during the simulation. Due to the inductive effect of the solenoid circuit, solenoid current does not reach the critical value at which the magnetic force exceeds spring force and moves the plunger.

Figure 4.3 shows the model output for 10 Hz frequency 80 % duty value PW modulated input signal. According to the figure, the valve cannot be closed with the given signal. Similar to the opening case, this can also be seen by the current output since there is no minima or maxima occurrence during the simulation. Due to the inductive effect of the solenoid circuit, solenoid current does not reach the critical at which the

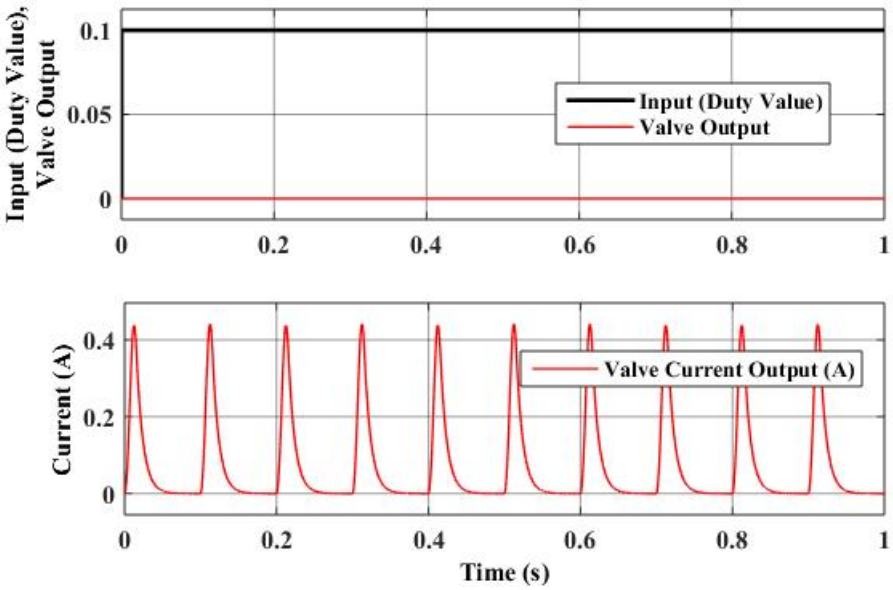

Figure 4.2: Valve Model Output for 10 Hz 10 % Duty Value Input

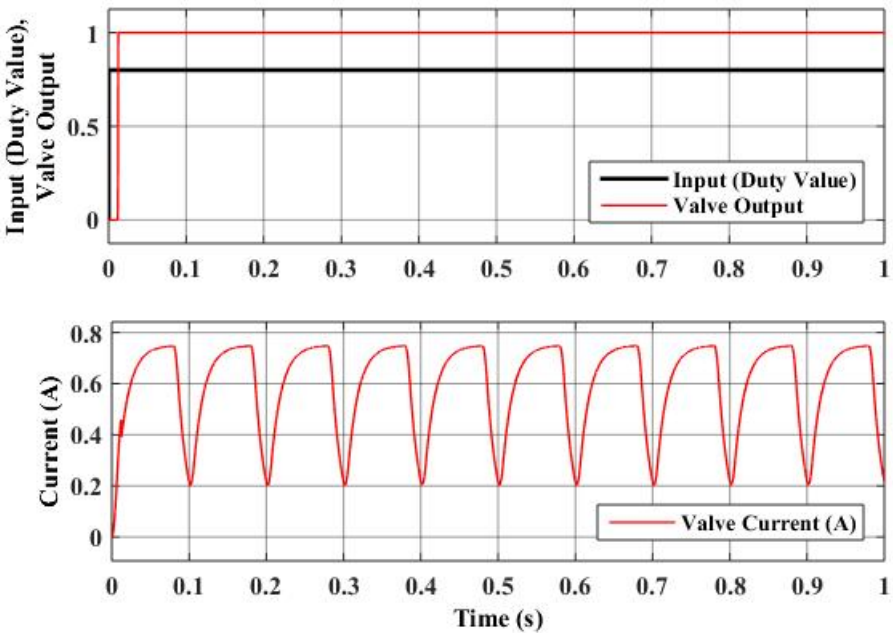

Figure 4.3: Valve Model Output for 10 Hz 80 % Duty Value Input

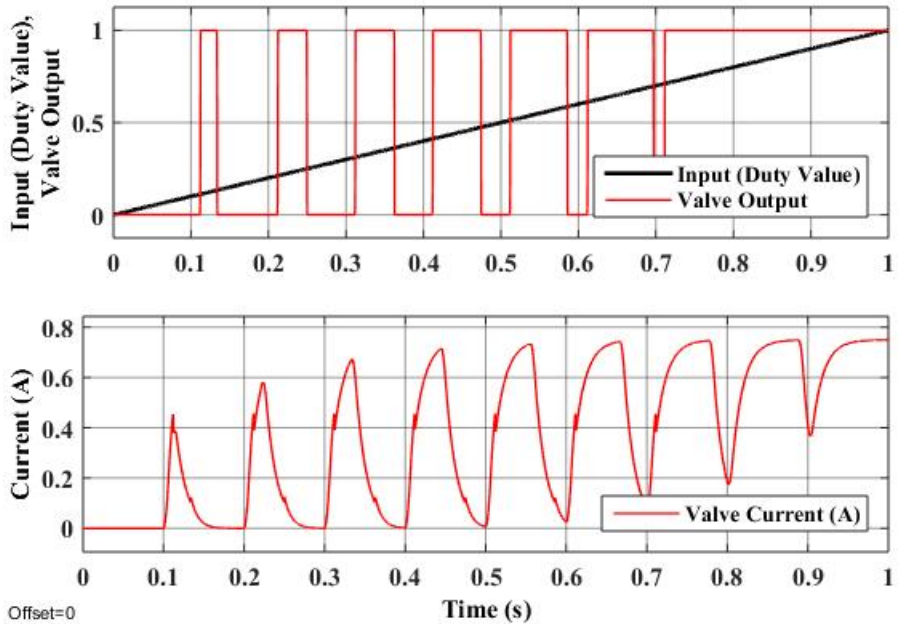

Figure 4.4: Valve Model Output for 10 Hz Ramp Input

spring force exceeds magnetic force and moves the plunger.

Figure 4.4 shows the model output for 10 Hz frequency and changing duty valued PW modulated input signal. This simulation is obtained by the ramp input type of duty value, it changes from 0 to 1 in 1 second. Thus, the response interval for the duty value can be seen in this simulation.

When Figures 4.2, 4.3 and 4.4 are investigated, it is observed that for 10 Hz frequency there are minimum and maximum duty values that are applicable on the valve. Approximately, for the duty values lower than 0.1, the valve cannot be opened and for the duty values higher than 0.65, the valve cannot be closed.

Figure 4.5 shows the model output for 5 Hz frequency and 0.1 duty value PW modulated input signal. Contrary to the 10 Hz case, the valve output is achieved for the same duty value input. This is due to the fact that the PWM period is doubled after the open command time interval is doubled. As a result, the time interval of the valve opening becomes smaller than the time interval of the open command.

Figure 4.6 shows the model output for 5 Hz frequency and 0.8 duty value PW modulated input signal. Contrary to the 10 Hz case, the valve output is achieved for the same duty value input. This is due to the fact that the PWM period is doubled after

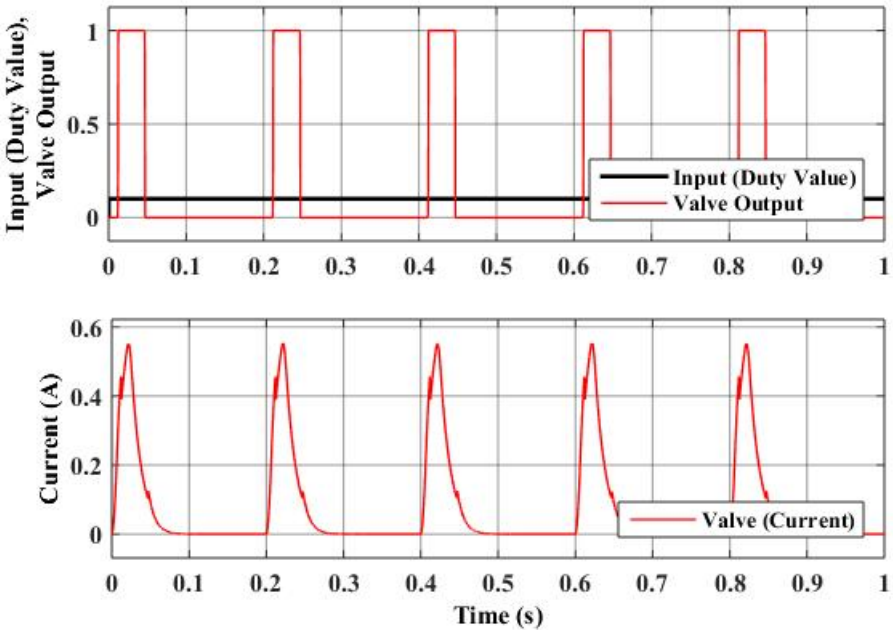

Figure 4.5: Valve Model Output for 5 Hz 10 % Duty Value Input

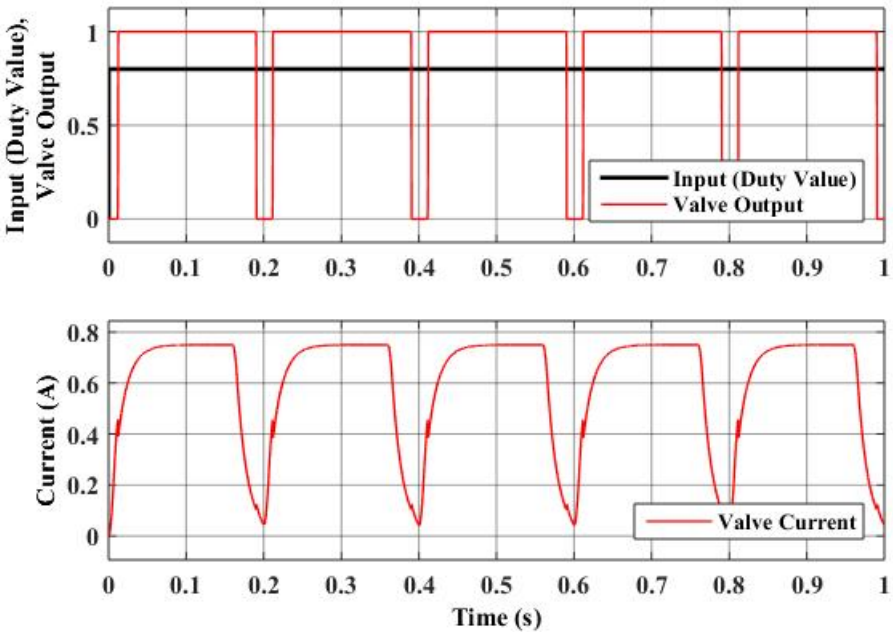

Figure 4.6: Valve Model Output for 5 Hz 80 % Duty Value Input

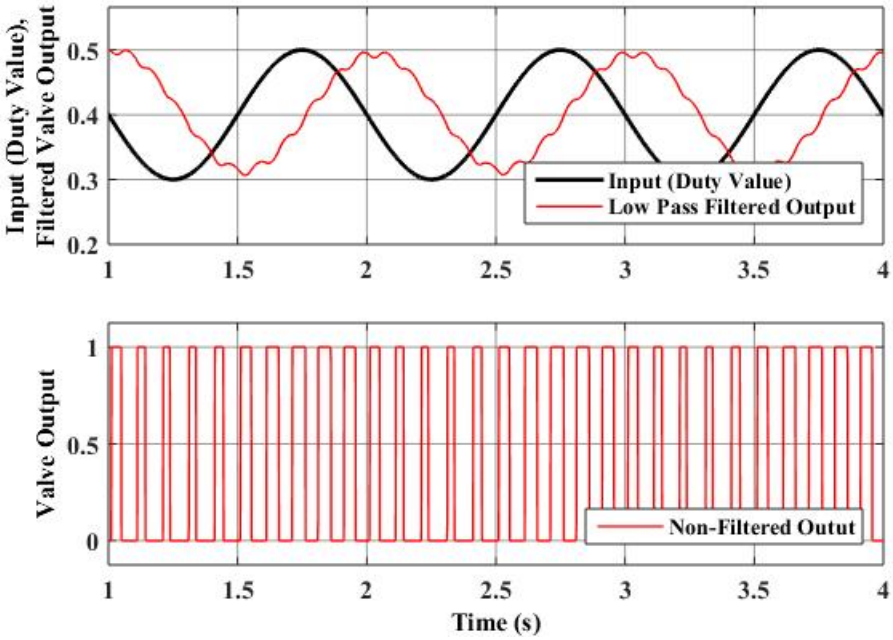

Figure 4.7: Model Output for 1 Hz Sinusoidal Input - 10 Hz PWM frequency

the open command time interval is doubled. As a result, the time interval of valve closing is smaller than the time interval of the open command.

It is inferred from Figures 4.2 and 4.5 that the lower frequency PW modulator resulted with smaller minimum duty value limit. Similarly Figures 4.3 and 4.6 show that lower frequency PW modulator resulted with greater maximum duty value limit.

When only duty cycle limits are taken into consideration, the low frequency PWM gives the best result. However, using the low frequency PWM results in poor tracking performance with high frequency inputs. Figures 4.7, 4.8 and 4.9 give the model output graphs for 1 Hz sinusoidal input and 10, 5 and 2 Hz PWM frequency, respectively. Model outputs are given as both direct thruster output and low pass filtered output. By using the low pass filter, input and output relationship viewed easily. Block diagram of this simulation given in Figure 4.10.

When figures 4.7, 4.8 and 4.9 are examined higher PWM resulted with better tracking performance. Results are matching with general rule of thumb that a frequency of the actuator should be at least 4 to 5 times greater than input frequency. A sinusoidal input which has 1 Hz frequency is applied to the system and 2 Hz PWM couldn't track the input. However 5 Hz frequency was able to track the input and 10 Hz frequency was

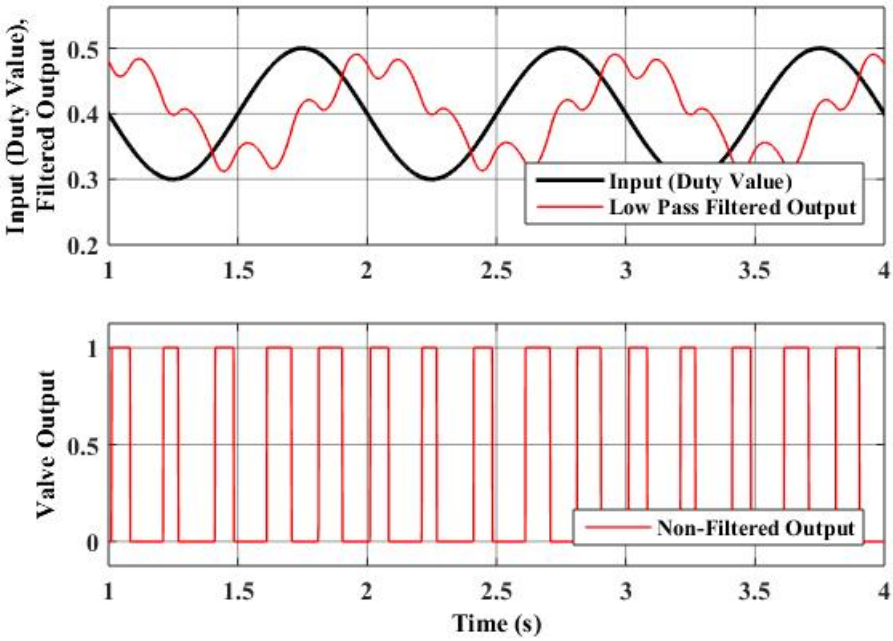

Figure 4.8: Model Output for 1 Hz Sinusoidal Input - 5 Hz PWM frequency

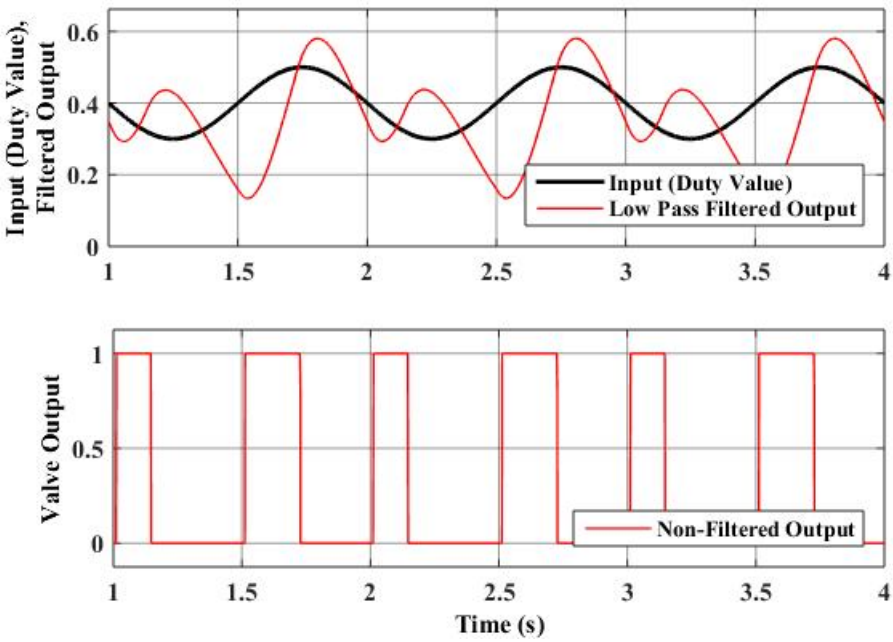

Figure 4.9: Model Output for 1 Hz Sinusoidal Input - 2 Hz PWM frequency

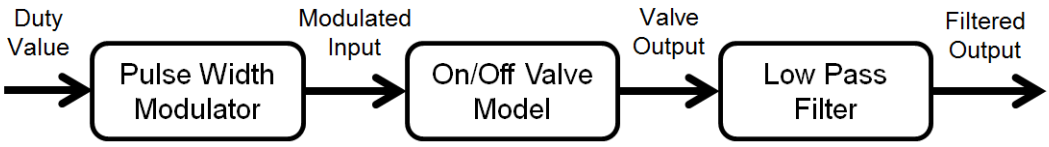

Figure 4.10: Block Diagram of Valve Simulation

even much better for input tracking.

Simulations made in this section show the limitations of the PWM frequency selection. According to the simulations, lower frequency is advantageous to obtain greater duty value working intervals. On the other hand, higher frequency PWM is better for tracking higher frequency inputs.

4.1.2 Calculation of PWM Frequency

In this section, a method for PWM frequency selection is presented. As explained in the previous section, there are restrictions while selecting the PWM frequency. PWM frequency affects the limits of duty cycle and the bandwidth of the system.

One of the methods for PWM frequency selection is based on trial and error. For this method, PWM applied signal model or test setup can be used. Output can be examined by changing the input PWM frequency. However, in this work PWM frequency selection will be formalized.

When modulated signal is applied, the minimum duty cycle limit occurs. This is due to the fact that the time interval of the applied open signal for one cycle is less than the opening time interval of the valve. Thus, the minimum time interval for the open command must be greater than the opening time interval. For the highest possible PWM frequency, below formula guarantees the opening of the valve for the selected minimum duty cycle limit.

$$T_{PWM} > \frac{1}{DC_{min}} T_{open} \tag{4.1}$$

Similar to the minimum duty cycle case, the maximum duty cycle limit occurs when the time interval of the applied close signal for one cycle is less than the closing time interval of the valve. Thus, the minimum time interval for the closing time interval must be greater than the closing time interval of the solenoid valve. For the highest possible PWM frequency, below formula guarantees the closing of the valve for the selected maximum duty cycle limit.

$$T_{PWM} > \frac{1}{1 - DutyCycle_{max}} T_{close} \tag{4.2}$$

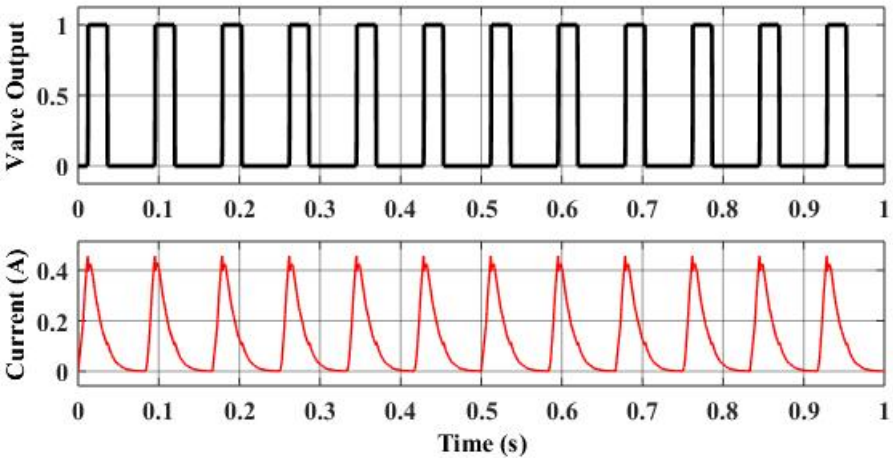

Figure 4.11: Model Output for 15 % Duty Value - 12 Hz PWM frequency

And PWM frequency:

$$f_{PWM} = \frac{1}{T_{PWM}} \tag{4.3}$$

Selection of the duty cycle limits is related to the overall system requirements. Phase plane analysis might be useful to determine the required minimum and maximum duty cycle limits. As mentioned before, the minimum and the maximum duty cycle limits correspond to the dead band and the saturation of the system, respectively . For example for this test system, 15% and 60% duty cycle limits and PWM frequency is calculated.

According to Equation 4.1 for 15 % duty cycle limits PWM frequency:

$$T_{PWM} > 80 \tag{4.4}$$

According to Equation 4.2 for 60 % duty cycle limits PWM frequency:

$$T_{PWM} > 75 \tag{4.5}$$

Since greater PWM period satisfies both of the duty cycle requirements, for 80 ms PWM period, 12 Hz PWM frequency is selected according to Equation 4.3.

Figures 4.11 and 4.12 show model outputs for 0.15 and 0.6 duty value inputs with 12 Hz PWM, respectively. According to the figures, valve is able to give modulated response for the selected duty cycle limits.

Figure 4.13 shows model output for 2 Hz sinusoidal input for 12 Hz PWM. As seen

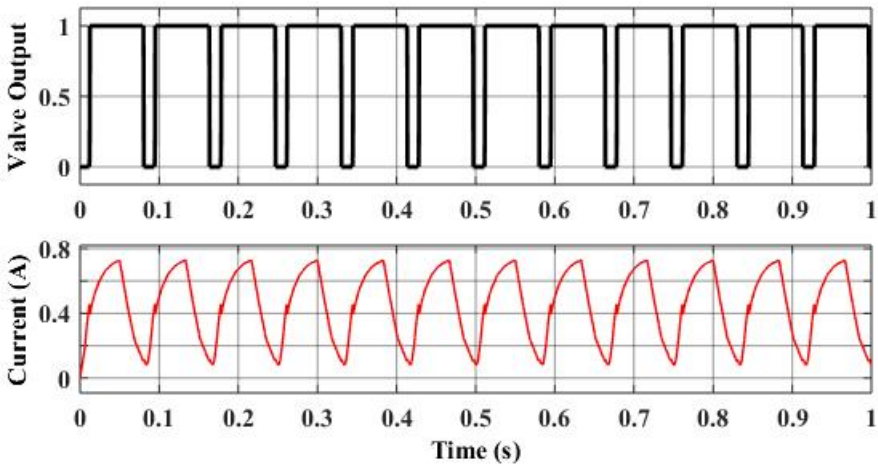

Figure 4.12: Model Output for 60 % Duty Value - 12 Hz PWM frequency

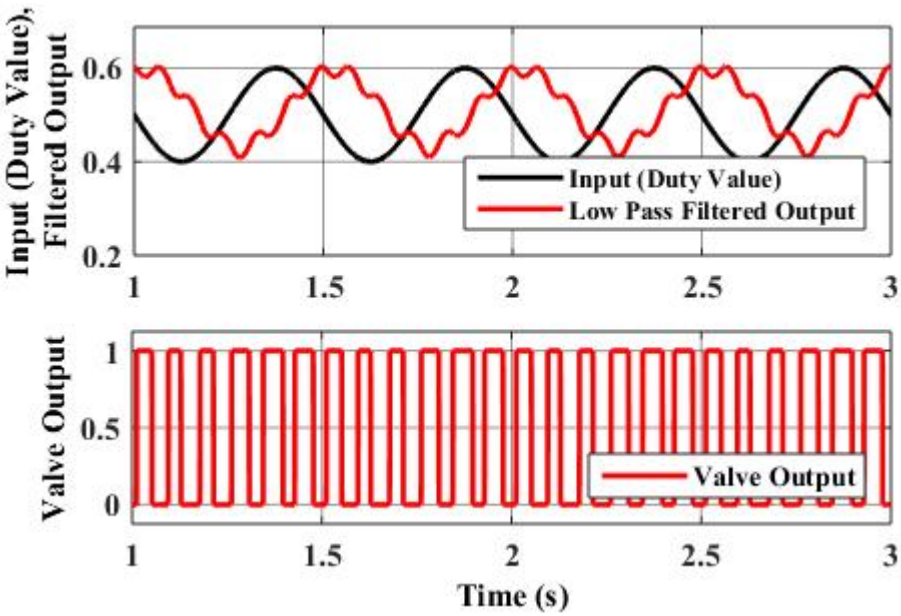

Figure 4.13: Model Output for 2 Hz Sine Input - 12 Hz PWM frequency

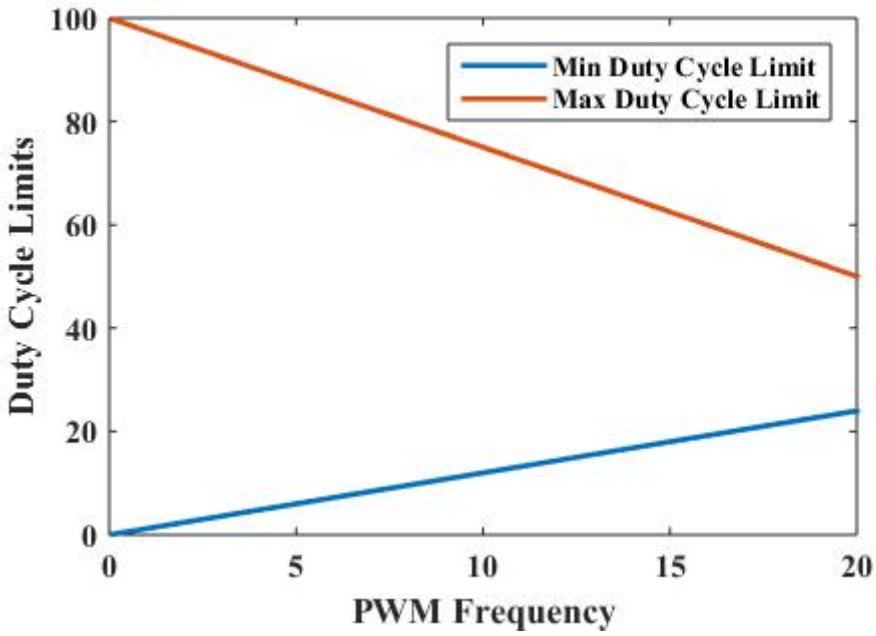

Figure 4.14: Frequency - Duty Value Limit Comparison

from the figure, 12 Hz PW modulated model can track 2 Hz sinusoidal input as expected.

Figure 4.14 shows the comparison of the minimum and the maximum duty cycle limits with PWM frequency. The figure is obtained from the obtained duty value calculation equations. As can be inferred from the figure that an increase in PWM frequency results in a shorter range of applicable duty cycle values.

4.1.3 Performance Result of the Modulated Thruster

In this section of the chapter, performance of the PW modulated is investigated. Discrepancies between the aimed and the gained output are examined. Modifications are applied on the model according to the discrepancies.

Figures 4.15, 4.16 and 4.17 show valve output for 0.15, 0.45 and 0.60 duty value inputs, respectively. According to the figures, average response of the valve is greater than the input duty value.

The main reason of the difference between the input and the average output is found as the time interval difference between the opening and the closing times. In section

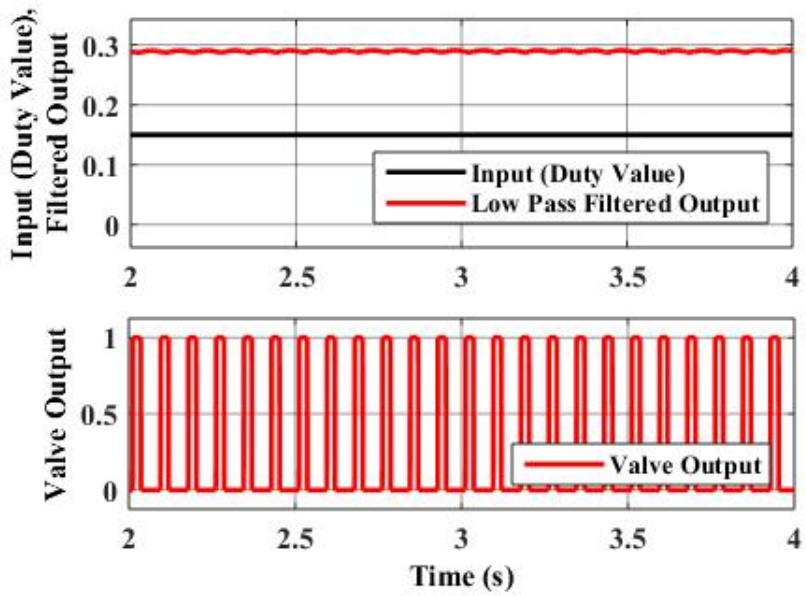

Figure 4.15: Valve Model Output 15 % Duty Value - 12 Hz PWM

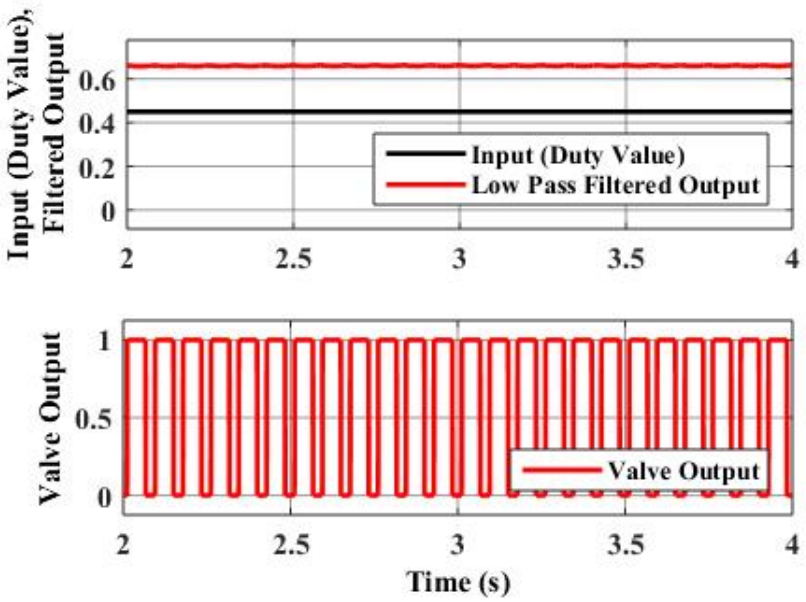

Figure 4.16: Valve Model Output 45 % Duty Value - 12 Hz PWM

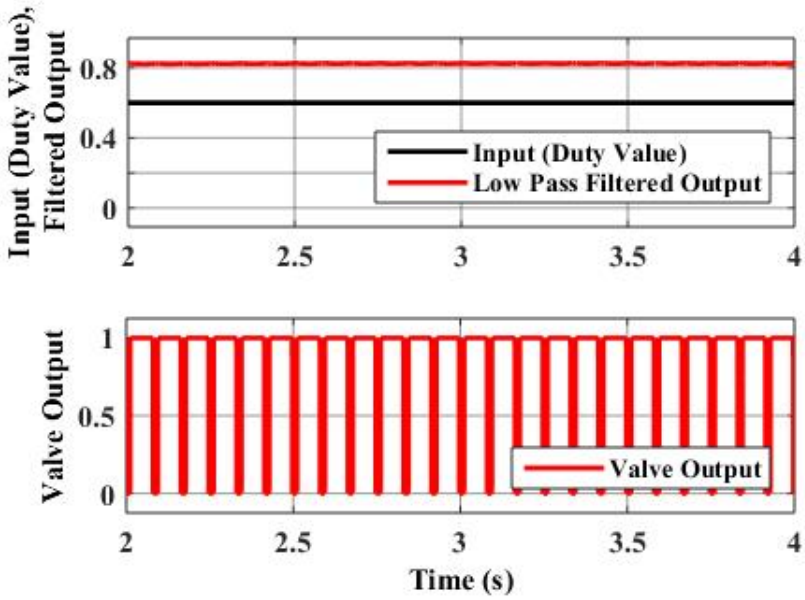

Figure 4.17: Valve Model Output 60 % Duty Value - 12 Hz PWM

3, the opening time interval is calculated as 12 ms. However, the closing time interval is calculated as 30 ms. Thus, when the open command is applied, the valve starts its motion 12 ms after the command. Similarly, when the close command is applied, the valve starts its closing motion 30 ms after the command. As a result, the valve stays 18 ms more open state than desired throughout one cycle.

For the selected PWM frequency, the desired open valve duration can be calculated using the below equation.

$$t_{OpenValveDuration} = T_{PWM} * DV \tag{4.6}$$

For 12 Hz PWM frequency, when 0.45 duty value input is applied, desired open valve duration according to Equation 4.6 is

$$t_{OpenValveDuration} = 37.5ms \tag{4.7}$$

However, it is known that an extra of 18 ms valve open duration is added by valve characteristics to the desired value and the valve open time duration becomes 55.5 ms. Thus, Equation 4.6 can be modified as below to calculate the output duty value.

$$DV = \frac{t_{OpenValveDuration}}{T_{PWM}} \tag{4.8}$$

According to the above equation, the output duty value becomes 0.66. This calculated output duty value overlaps with the result of Figure 4.16. Thus, the conclusion might

be that a duty value is always added to the modulated response equal to $\frac{18}{T_{PWM}}$. The minimum and maximum duty values become greater than the previously calculated ones.

4.2 Closure

In this chapter, a methodology for frequency selection of PWM is proposed. Other than the system requirements, valve dynamics are considered during the frequency selection. First, the relationship between valve opening-closing time intervals, PWM frequency and upper/lower duty cycle limits are illustrated. It is concluded that in order to obtain greater range of duty cycle range without exceeding the lower and the upper duty cyle limits, lower PWM frequency should be selected. On the other hand, it is shown that the lower PWM frequency results with lower actuator bandwidth and thruster cannot track high frequency duty value inputs. In this work, the highest possible PWM frequency is calculated, which satisfies the duty cycle limits. At last, the difference between the duty cycle input and the average output is mentioned. It is concluded that this difference came from the difference between the time intervals of opening and closing motion of a solenoid valve. Calculation method of difference between the duty value input and the average output is also presented.

CHAPTER 5

CONTROLLER DESIGN

5.1 Introduction

In this chapter, controllers are designed for single axis angle control and stabilization of inverted pendulum. PW modulated on/off solenoid valve is treated as a linear actuator and linear control methods are applied.

Designed controllers are verified using dynamical model and PW modulated thruster model. Discrepancies originated from the on/off actuator dynamics are examined and the performance of the PWM scheme are discussed. Results are compared with the unmodulated controller.

5.2 Single Axis Controller Design

PW Modulated thrusters are first tried on the single axis control application. Single axis angle control scheme is the simplified version of the attitude control application. Designed controller and performance results provide an insight for attitude control application.

Figure 5.1 shows the schematic of a single axis control application. It is a mass attached to a revolute joint and there are two oppositely placed thrusters on the mass. Revolute joint enhances single axis freedom and two oppositely thrusters create control torque on the freely rotating mass. Angular position of the mass is the feedback signal of the closed loop system.

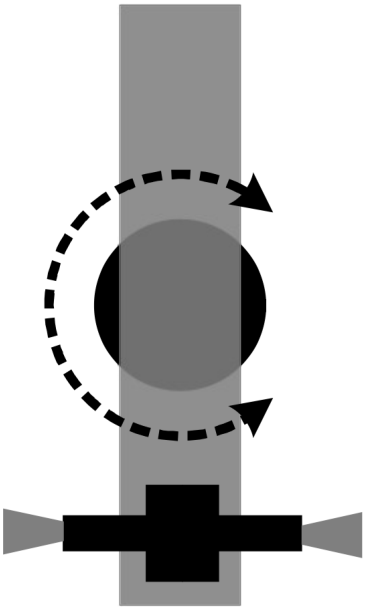

Figure 5.1: Single Axis Angle Control Application Schematic

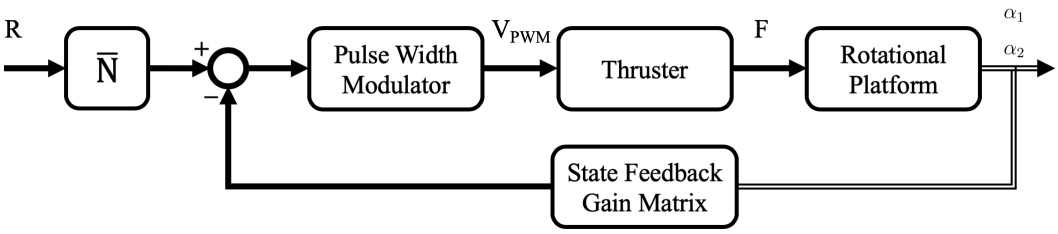

Figure 5.2: Single Axis Angle Control Application Block Diagram

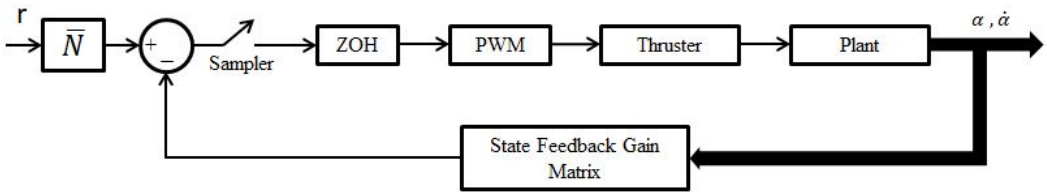

Figure 5.3: Block Diagram with Discrete Dynamics

In Figure 5.1, dynamics related to discretization due to PWM scheme is omitted. However, to be able to apply the modulated input, control signal is sampled and held with the PWM frequency. The modified block diagram which includes these dynamics is given in Figure 5.3.

Due to the low dynamical performance of the on/off valves, PWM frequency is kept low. Thus, the sampling period is high when compared with the system dynamics. To be able to obtain better response, discrete controller is designed by considering the low frequency sample and the hold effect.

In this section, dynamical model of the single axis application is obtained first. Secondly, linear controller is designed and lastly the results are examined. Figure 5.2 shows the block diagram of the application. As seen from the block diagram, PW modulated thruster actuated rotational platform is controlled by the state feedback controller.

5.2.1 Dynamical Model

Dynamical model of the single axis test setup is based on a rotational inertia and torque on it. Equation of motion is

$$J_{rod}\ddot{\alpha} = T_{thrust} \tag{5.1}$$

Torque generated by the thruster is

$$T_{thrust} = Fr_{rod} \tag{5.2}$$

Equation of motion becomes

$$J_{rod}\ddot{\alpha} = Fr_{rod} \tag{5.3}$$

Table 5.1: Single Axis Test Setup Parameters

Parameters	
J_{rod}	0.2 kgm^2
F	2 N
r_{rod}	0.25 m

By taking Laplace Transform of the equation of motion, transfer function of the system can be obtained as below:

$$G(s) = \frac{\alpha(s)}{u(s)} = \frac{Fr}{Js^2} \tag{5.4}$$

State space form of the equation of motion is

$$\begin{bmatrix} \dot{\alpha_1} \\ \dot{\alpha_2} \end{bmatrix} = \begin{bmatrix} 0 & 1 \\ 0 & 0 \end{bmatrix} \begin{bmatrix} \alpha_1 \\ \alpha_2 \end{bmatrix} + \begin{bmatrix} 0 \\ F\frac{r_{rod}}{J_{rod}} \end{bmatrix} u \tag{5.5}$$

Table 5.1 shows the test setup parameters for the single axis motion. By inserting these parameters into the transfer function and the state space form equations, below equations are obtained.

$$G(s) = \frac{\alpha(s)}{u(s)} = \frac{1.6}{s^2} \tag{5.6}$$

$$\begin{bmatrix} \dot{\alpha_1} \\ \dot{\alpha_2} \end{bmatrix} = \begin{bmatrix} 0 & 1 \\ 0 & 0 \end{bmatrix} \begin{bmatrix} \alpha_1 \\ \alpha_2 \end{bmatrix} + \begin{bmatrix} 0 \\ 1.6 \end{bmatrix} u \tag{5.7}$$

5.2.2 Discrete-Time Model

Discrete model is also constructed based on the used PWM frequency. According to Figure 5.3, pulse transfer function changes with the addition of the zero order hold. Transfer function of the zero order hold is

$$G(s) = \frac{1 - e^{-Ts}}{s} \tag{5.8}$$

Pulse transfer function is

$$G(s) = \frac{1 - e^{-Ts}}{s}\frac{1.6}{s^2} \tag{5.9}$$

Z transform of pulse transfer function is calculated as

$$G(z) = Z\left(\frac{1-e^{-Ts}}{s}\frac{1.6}{s^2}\right) = (1-z^{-1})Z\left(\frac{1.6}{s^3}\right) \tag{5.10}$$

$$G(z) = 1.6(1-z^{-1})\frac{T^2 z^{-1}(1+z^{-1})}{2(1-z^{-1})^3} \tag{5.11}$$

$$G(z) = 0.8T^2\frac{z+1}{z^2-2z+1} \tag{5.12}$$

For 10 Hz PWM frequency discrete time transfer function is given as below.

$$G(z) = \frac{0.008z+0.008}{z^2-2z+1} \tag{5.13}$$

State space form of the discrete time transfer function is determined.

$$\begin{bmatrix}\alpha_1(k+1)\\ \alpha_2(k+1)\end{bmatrix} = \begin{bmatrix}1 & 0.1\\ 0 & 1\end{bmatrix}\begin{bmatrix}\alpha_1(k)\\ \alpha_2(k)\end{bmatrix} + \begin{bmatrix}0.008\\ 0.16\end{bmatrix}u \tag{5.14}$$

5.2.3 State Feedback Controller Design

In this section, state feedback controller, a linear control method, is designed. States were set in the previous section as the angular position and the angular velocity of the rotating rod. When the state feedback is applied, input thrust force becomes

$$F_{thrust} = -\mathbf{K}\begin{bmatrix}\alpha_1\\ \alpha_2\end{bmatrix} \tag{5.15}$$

where **K** is the state feedback gain matrix. Thus, the overall state space form becomes

$$\begin{bmatrix}\dot{\alpha_1}\\ \dot{\alpha_2}\end{bmatrix} = \left(\begin{bmatrix}0 & 1\\ 0 & 0\end{bmatrix} - \begin{bmatrix}0\\ \frac{r_{rod}}{J_{rod}}\end{bmatrix}\mathbf{K}\right)\begin{bmatrix}\alpha_1\\ \alpha_2\end{bmatrix} \tag{5.16}$$

The term in the parenthesis in the above equation determines the characteristics of the closed loop system. Eigenvalues of this term must be equal to the desired pole locations. Calculation of matrix **K** to satisfy the requirement of the eigenvalues can be done by using Ackermann's formula.

The Ackermann's formula related to this system given as below equation.

$$\mathbf{K} = \begin{bmatrix} 0 & 1 \end{bmatrix} \begin{bmatrix} \mathbf{B} & \mathbf{AB} \end{bmatrix}^{-1} \phi(\mathbf{A}) \tag{5.17}$$

$\phi(\mathbf{A})$ is given below. In the below equation α_1 and α_2 are the coefficients of the desired characteristic equations.

$$\phi(\mathbf{A}) = \mathbf{A}^2 + \alpha_1 \mathbf{A} + \alpha_2 \mathbf{I} \tag{5.18}$$

5.2.4 State Feedback Controller Design is Discrete Domain

Similar to the continuous case, state feedback controller gain is also calculated for the model constructed in discrete domain.

$$F_{thrust} = -\mathbf{K} \begin{bmatrix} \alpha_1(k) \\ \alpha_2(k) \end{bmatrix} \tag{5.19}$$

where **K** is the state feedback gain matrix. Thus, the overall state space form becomes

$$\begin{bmatrix} \alpha_1(k+1) \\ \alpha_2(k+1) \end{bmatrix} = \left(\begin{bmatrix} 1 & 0.1 \\ 0 & 1 \end{bmatrix} - \begin{bmatrix} 0.008 \\ 0.16 \end{bmatrix} \mathbf{K} \right) \begin{bmatrix} \alpha_1(k) \\ \alpha_2(k) \end{bmatrix} \tag{5.20}$$

Feedback gain matrix K is calculated according to the desired eigen-values of the discrete time state space system. **K** is found by Ackermann's formula. The related equation is given in 5.17 and 5.18.

5.2.5 Simulation Results

In this section, results of the single axis control simulation are presented. Simulations are carried out with different control gains and schemes and the results are compared. Combinations of different PWM frequencies and controller resulting in different system bandwidths are tried.

Calculations of natural frequencies satisfying the required system bandwidth are done using the below equation. The damping ratio is selected as 1 to obtain results without

overshoot.

$$w_n = \frac{w_b}{\sqrt{1 - 2\zeta^2 + \sqrt{(1 - 2\zeta^2)^2 + 1}}} \tag{5.21}$$

Eigenvalues are calculated with the below formula.

$$s_{1,2} = -\zeta w_n \tag{5.22}$$

For the discrete case, eigenvalue is converted to z domain using

$$z_{1,2} = e^{s_{1,2}ts} \tag{5.23}$$

Firstly, simulation is carried out for 10 Hz PWM frequency and 1 Hz controller bandwidth. Controller is designed for both continuous and discrete domains.

Figure 5.4 shows the results of the angular position simulation for three different cases. One of them is without using any modulator. Other two are with modulator and gains calculated for both continuous and discrete cases. According to the figure, all cases have similar results. However, the case modulator with continuous controller is oscillatory around the desired position. For this case, sample and hold effect of the modulator are not taken into consideration and the discrete dynamics are omitted while designing the controller. As a result, the controller response is poorer than other cases.

Figure 5.5 shows the thruster fire comparison between no modulation and modulation with the discrete controller cases. According to the figure, the number of thruster fires for the required motion is much higher for the un-modulated case. Higher number of fires results with higher fuel and battery power consumption and early valve wear. Propellant consumption comparison is given in Figure 5.6.

Figure 5.7 shows the angular position simulation result when 0.5 Hz sine signal applied. The system can track the reference input for -3 dB bandwidth rule.

Figure 5.8 shows the angular position simulation results for 10 Hz PWM frequency and 2 Hz system bandwidth. As seen from the figure, only discrete controller with

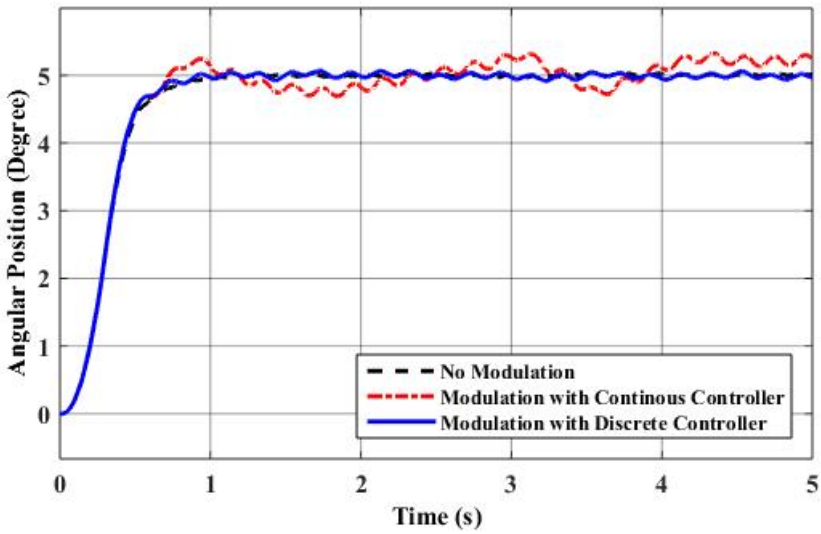

Figure 5.4: Angular Position Simulation - 10 Hz PWM and 1 Hz Bandwidth Frequency

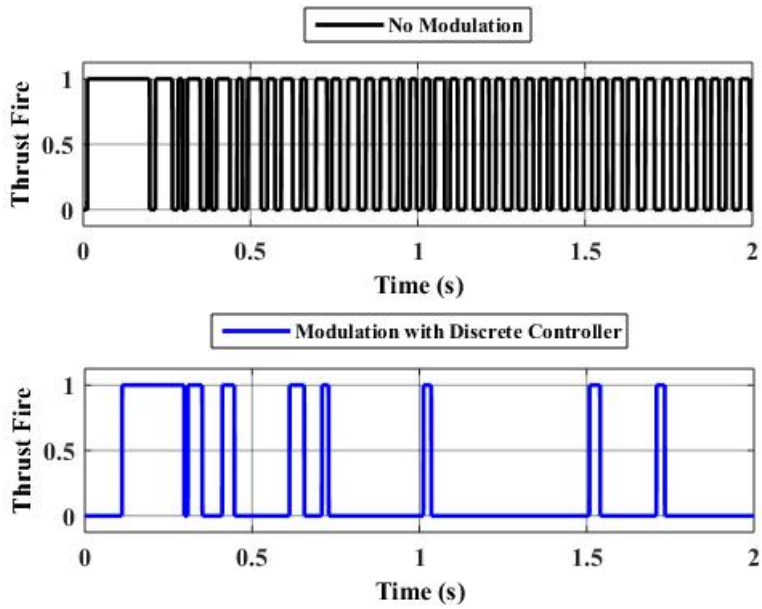

Figure 5.5: Thruster Fire Comparison

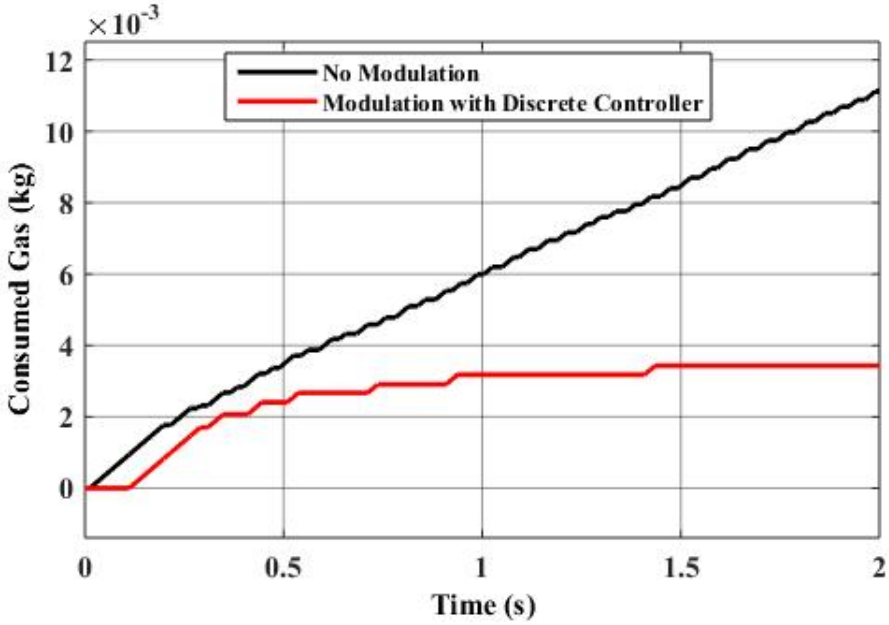

Figure 5.6: Propellant Consumption Comparison

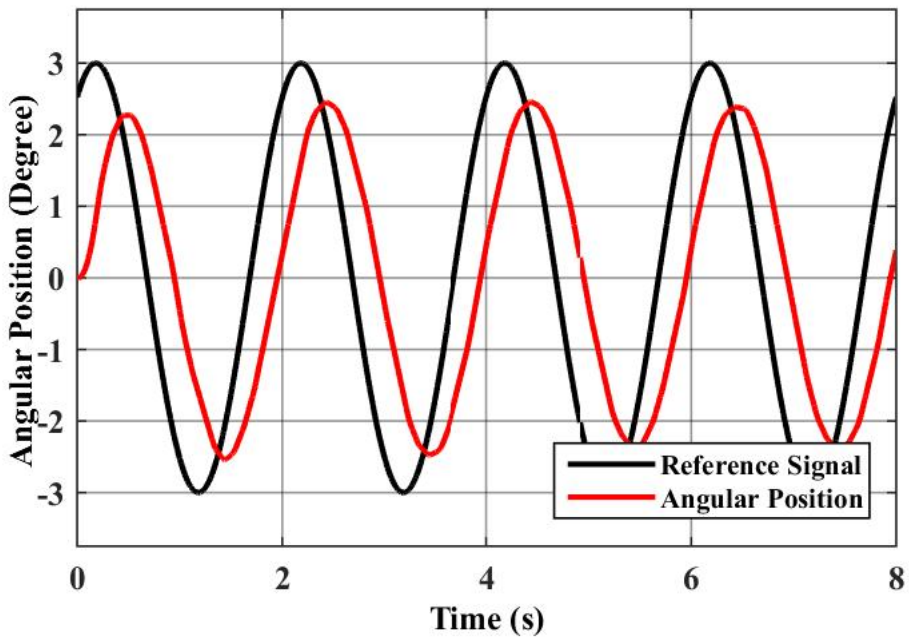

Figure 5.7: 0.5 Hz Bandwidth Simulation

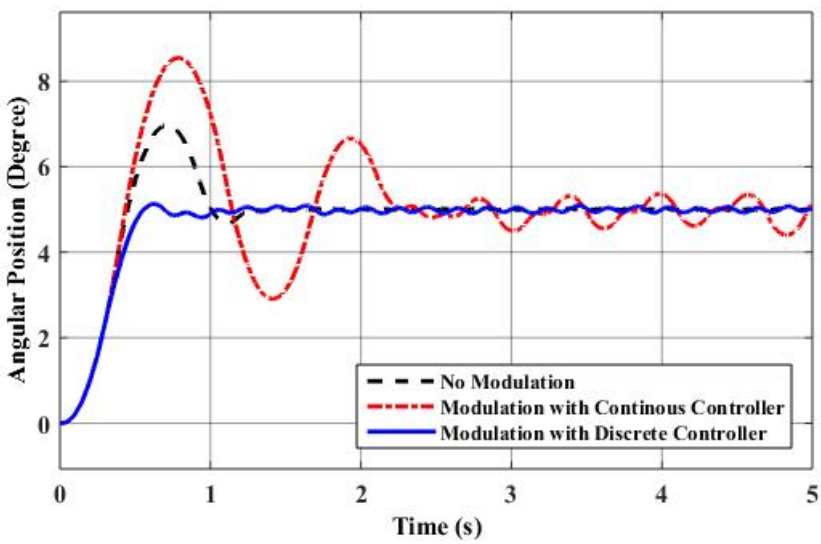

Figure 5.8: Angular Position Simulation - 10 Hz PWM and 2 Hz Bandwidth Frequency

modulator has resulted with desired performance. System bandwidth frequency and PWM frequency or switching frequency of bang bang action are closer.

Figure 5.9 shows the simulation results for 5 Hz PWM frequency and 5 Hz system bandwidth. According to the figure, continuous controller case becomes unstable.

Throughout this section, controllers are designed for small angle bandwidth requirements. Designing the controller for small angles may result actuator saturation for higher angular position commands. The saturation behavior may disrupt controller performance. One way of preventing saturation might be designing the controller by considering high angular position commands. However, if for small angle higher bandwidth is required, this solution could not satisfy all of the requirements. Another way of preventing saturation is filtering the commands by proper rate limiter. Thus, the commands will not be applied as a step input and saturation will be prevented. Figure 5.10 shows the high angle command angular position simulation results for both rate limited and without rate limited cases. As seen from the figure, using rate limiter prevents undesired overshoot.

A simulation is also done for a designed controller according to 0.7 damping ratio and 1 Hz Bandwidth specifications. Figure 5.11 shows the angular position simulation result for this case. Regarding the performance, overshoot is obtained as expected.

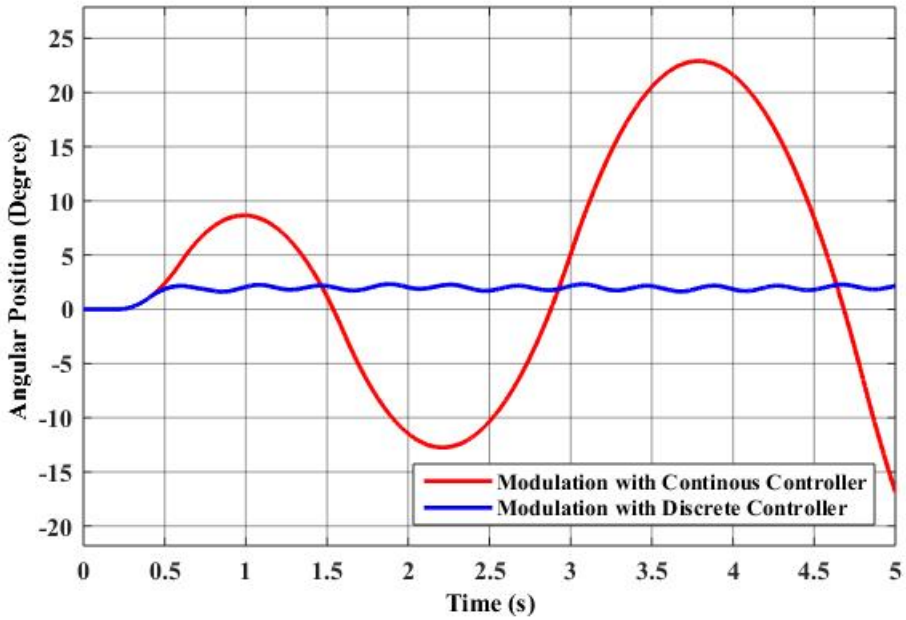

Figure 5.9: Angular Position Simulation - 5 Hz PWM and 5 Hz Bandwidth Frequency

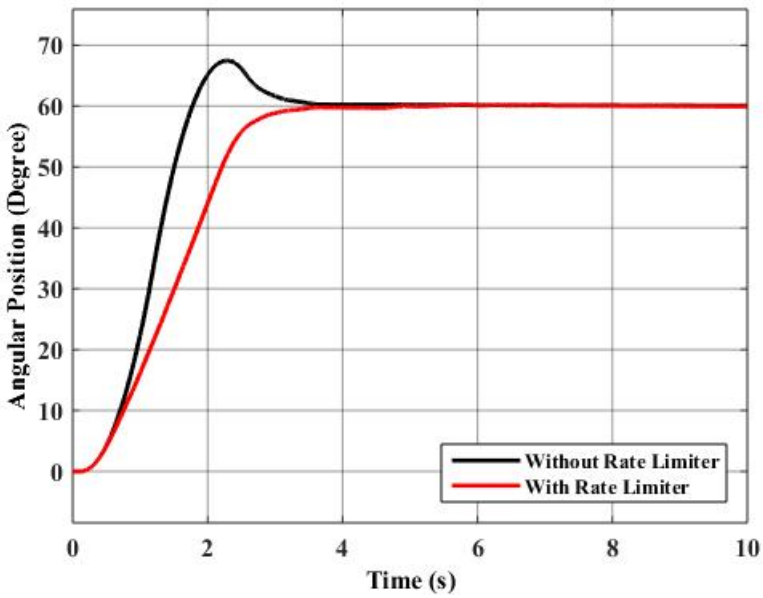

Figure 5.10: Angular Position Simulation - Rate Limiter Comparison

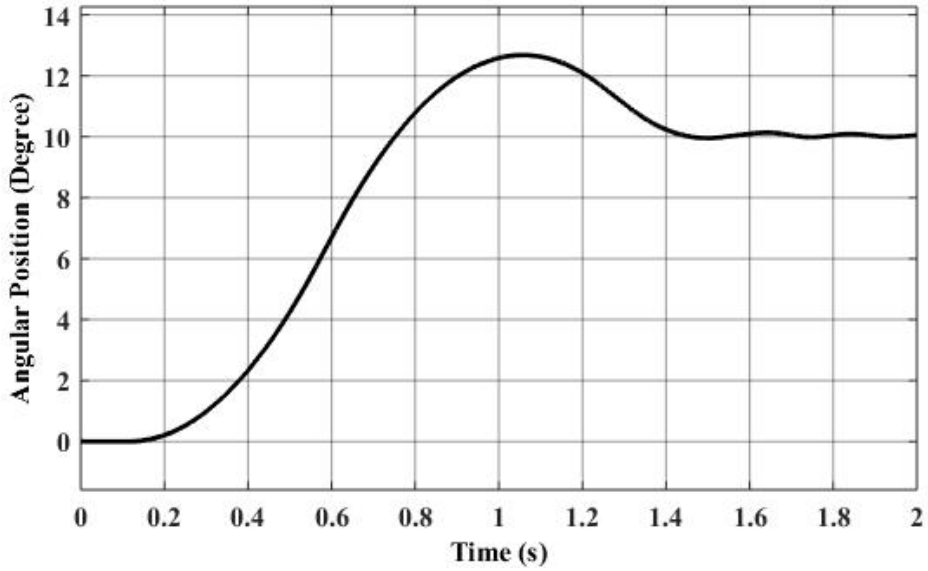

Figure 5.11: Angular Position Simulation - 0.7 Damping Ratio

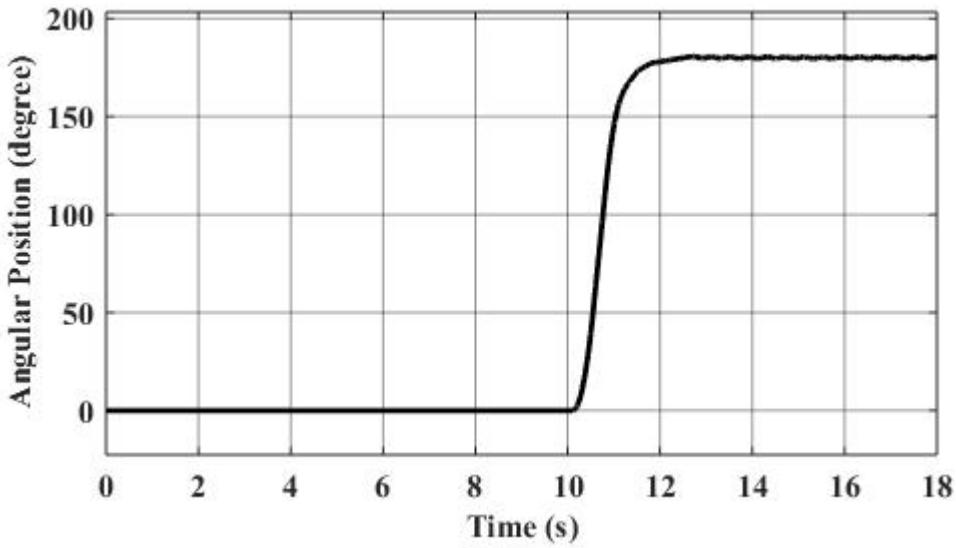

Figure 5.12: Angular Position Simulation for the Experiment Case

Lastly Figure 5.12 shows the angular position when 180 degrees angle command is applied. According to the figure, it takes 2 seconds for the single axis platform to reach the desired position. This case will be compared with the experiments.

5.3 Rotary Inverted Pendulum Application

Now, PW Modulated thrusters are used on the rotary inverted pendulum application. As explained in Chapter 2, inverted pendulum is a inherently unstable, under-actuated control problem. So, thruster actuated rotary inverted pendulum application will give insight on any application with on/off actuated, unstable and under-actuated control problem. In addition to that, thruster actuated inverted pendulum application has a similar dynamics with the attitude control of a satellite with slosh dynamics. Hence, designed controller scheme and the results are also beneficial for attitude control with slosh dynamics problem.

In this section, firstly the dynamical model of the rotary inverted pendulum is constructed and the equation of motion is obtained. Secondly, linear controller is designed and lastly the results are examined.

5.3.1 Dynamical Model of the Rotary Inverted Pendulum

In this sub-section, the equation of motion is obtained by constructing the dynamical model of the rotary inverted pendulum. Lagrangian method is used to obtain the rotary inverted pendulum dynamics.

Figure 5.13 shows the free body diagram of the rotary inverted pendulum. As seen from the free body diagram, α is defined as the rod angle and θ is defined as the pendulum angle. Rotary inverted pendulum is a spatial system, which means that the system does not move on a single plane. Although the system is spatial, it can be separated as two planar systems. Since centrifugal forces are not effective on the control action of the system, they are not considered on the free body diagram and are not going to be taken into consideration.

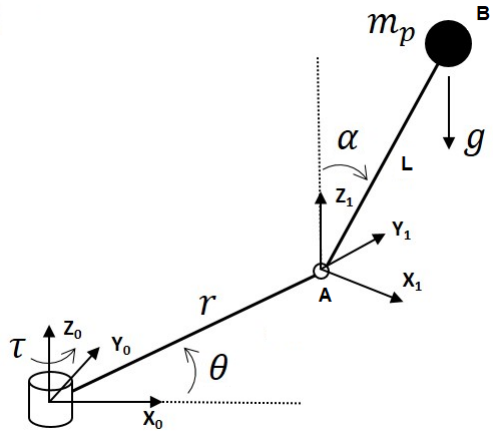

Figure 5.13: Free Body Diagram of the Rotary Inverted Pendulum

Using the free body diagram, the kinematic equations for point A are

$$x_A = r\theta \tag{5.24}$$

$$\dot{x_A} = r\dot{\theta} \tag{5.25}$$

Kinematic equations for point B with respect to point A are

$$x_{BA} = Lsin\alpha \tag{5.26}$$

$$\dot{x_{BA}} = Lcos\alpha\dot{\alpha} \tag{5.27}$$

$$y_{BA} = Lcos\alpha \tag{5.28}$$

$$\dot{y_{BA}} = -Lsin\alpha\dot{\alpha} \tag{5.29}$$

According to the relative motion principle

$$\dot{x_B} = r\dot{\theta} - Lcos\alpha\dot{\alpha} \tag{5.30}$$

$$\dot{y_B} = Lsin\alpha\dot{\alpha} \tag{5.31}$$

Mass moment of inertia of rod about mass center of rod is

$$J_{AO} = \frac{1}{12}m_{rod}r^2 \tag{5.32}$$

Mass moment of inertia of pendulum about mass center of pendulum is

$$J_B = \frac{1}{3} m_{pen} L^2 \tag{5.33}$$

To be able to use Lagrangian formulation, total kinetic and potential energies are calculated. Total kinetic energy is

$$T = \frac{1}{2} J_{AO} \dot{\theta}^2 + \frac{1}{2} m_{pen} (\dot{x}_B^2 + \dot{y}_B^2) + \frac{1}{2} J_B \dot{\alpha}^2 \tag{5.34}$$

Total potential energy is

$$V = m_{pen} g L cos\alpha \tag{5.35}$$

Then the Lagrangian function is

$$L = T - V \tag{5.36}$$

$$\begin{aligned} L = & \left(\frac{1}{2} J_{AO} + \frac{1}{2} m_{pen} r^2 \right) \dot{\theta}^2 + \left(\frac{1}{2} m_{pen} L^2 + \frac{1}{2} J_B \right) \dot{\alpha}^2 \\ & - m_{pen} r L cos\alpha \dot{\alpha} \dot{\theta} - m_{pen} g L cos\alpha \end{aligned} \tag{5.37}$$

Lagrange's equation:

$$\frac{d}{dt} \frac{dL}{d\dot{q}} - \frac{dL}{dq} + \frac{dD}{d\dot{q}} = Q \tag{5.38}$$

In the above equation, Q term is the input and for particular system it is the thrust force.

For $q = \theta$:

$$\frac{d}{dt} \left((J_{AO} + m_{pen} r^2) \dot{\theta} - m_{pen} r L cos\alpha \dot{\alpha} \right) = T_{thrust} \tag{5.39}$$

For $q = \alpha$:

$$\begin{aligned} & \frac{d}{dt} \Big((m_{pen} L^2 + J_B) \dot{\alpha} - m_{pen} r L cos\alpha \dot{\theta}) \\ & -(m_{pen} r L sin\alpha \dot{\alpha} \dot{\theta} + m_{pen} g L sin\alpha) = 0 \end{aligned} \tag{5.40}$$

For stabilization controller, linear control methods are applied. Non-linearity originated from the inverted pendulum kinematics is assumed as linear around the up-right position of the pendulum. Since balancing controller is working around the up-right position, it is a good assumption of this application.

Table 5.2: Inverted Pendulum Test Setup Parameters

Parameters	
J_{Ao}	0.2 kgm^2
T	1.25 Nm
r_{rod}	0.25 m
m_{pen}	25 g
L	0.135 m
J_B	0.0012 kgm^2

Linearized version of Equation 5.39:

$$(J_{AO} + m_{pen}r^2)\ddot{\theta} - m_{pen}rL\ddot{\alpha} = T \tag{5.41}$$

Linearized version of Equation 5.40:

$$(m_{pen}L^2 + J_B)\ddot{\alpha} - m_{pen}rL\ddot{\theta} - m_{pen}gL\alpha = 0 \tag{5.42}$$

Parameters related to Equations 5.41 and 5.42 are given in Table 5.2.

5.3.2 Minimum Torque Requirement for Balancing the Pendulum

In this section minimum torque requirement for balancing the pendulum near equilibrium position is calculated. So the sufficiency of torque generated by the thrusters is observed. Since the balancing controller is used near equilibrium position, peak torque is required for the limits of the determined near equilibrium position. The limit is determined as 10 degree from upper equilibrium position. So the required torque to balance the pendulum:

$$T_pen = m_{pen}sin(10)L = 5.86x10^{-4}Nm \tag{5.43}$$

Required acceleration at the point A:

$$\ddot{\theta} = T_{pen}/J_B = 0.4884rad/s^2 \tag{5.44}$$

And the required thruster torque is calculated below and it is lower than the obtained maximum thrust torque 1.25 Nm.

$$T = \ddot{\theta}J_{AO} = 0.09Nm \tag{5.45}$$

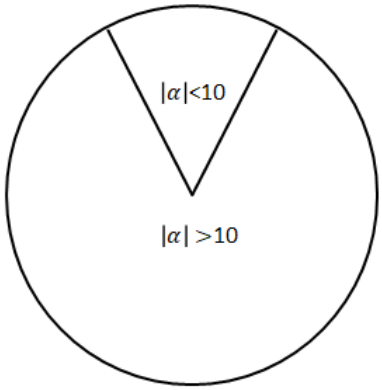

Figure 5.14: Switching Controller Scheme

5.3.3 Controller Design

In this section, design of the inverted pendulum controller is presented. Due to non-linearity of the pendulum motion, pendulum dynamics are linearized around upper equilibrium point. Thus, the pendulum motion is divided into two phases. One is the swing up motion and the other is the balancing motion. By this way, the balancing motion is accomplished using linear controller.

Figure 5.14 shows the phases of the controllers. For the case absolute value of the pendulum is smaller than 10 degrees, balancing controller is used. For the other case, swing controller is active. The transition between the controller phases is provided by a switch controller. In rest of this section, swing-up, balancing and switch controllers are presented.

5.3.3.1 Swing-up Controller

In this section, swing-up control algorithm is modeled. Swing-up controller is used to overcome the non-linearity of system. Since the system is linearized near the equilibrium position, swing up tries to bring the system near the equilibrium position. Energy control method is used for the swing-up action. This method calculates kinetic and potential energies of the pendulum. By knowing the total energy at the equilibrium position, the algorithm can apply necessary torque to the system [48].

The total energy of the pendulum system at any instant of the motion is

$$E = \frac{1}{2}J_{pen}\dot{\alpha}^2 + mgl(cos\alpha - 1) \tag{5.46}$$

Derivative of the energy equation is

$$\frac{dE}{dt} = J\dot{\alpha}\ddot{\alpha} - mgl\dot{\alpha}sin\alpha \tag{5.47}$$

Multiplying the equation of motion with the velocity of the pendulum and obtaining the energy change as

$$\frac{dE}{dt} = J\dot{\alpha}\ddot{\alpha} - mgl\dot{\alpha}sin\alpha = -m\ddot{\theta}l\dot{\alpha}cos\alpha \tag{5.48}$$

Using the above equation, energy of the pendulum can be controlled simply by changing the acceleration of the rod. This can be accomplished by applying necessary torque on the rod.

Controllability is lost when the coefficient of acceleration vanishes. This occurs when $\dot{\alpha}$ is zero or α is 180 degrees. To increase energy, the acceleration of the rod should be positive when the quantity $\dot{\alpha}cos\alpha$ is negative. Then, we can find the required acceleration of the rod as below [48].

$$\ddot{\theta} = k_{swing}(E - E_0)\dot{\alpha}cos\alpha \tag{5.49}$$

Above equation can adjust the required acceleration using real time energy as feedback value and when the total energy approaches the equilibrium energy, it lowers the acceleration. We should select an appropriate k_{swing} gain value for this system. k_{swing} is related with the torque limit and the allowing time for swing-up.

5.3.3.2 Balancing Controller

In this section, at the equilibrium point, balancing controller is designed. State feedback controller, a linear method, is designed. Firstly, the state space model is obtained. Then, the state feedback controller is designed. After that, the state observer is designed to observe some non-measurable states.

State Space Model of the Rotary Inverted Pendulum In this part, the state space model of the inverted pendulum is constructed. Equations 5.42 and 5.41 are formed as below, respectively.

$$c\ddot{\alpha} - b\ddot{\theta} - d\alpha = 0 \tag{5.50}$$

$$a\ddot{\theta} - b\ddot{\alpha} + d\dot{\theta} = T \tag{5.51}$$

where

$$a = J_{A0} + m_{pen}r^2 \tag{5.52}$$

$$b = lmr \tag{5.53}$$

$$c = \frac{4}{3}ml^2 \tag{5.54}$$

$$d = mgl \tag{5.55}$$

$$E = ac - b^2 \tag{5.56}$$

States are rod position, rod velocity, pendulum position and pendulum velocity. State space form of the equation of motion is

$$\begin{bmatrix} \dot{\alpha} \\ \dot{\theta} \\ \ddot{\alpha} \\ \ddot{\theta} \end{bmatrix} = \begin{bmatrix} 0 & 0 & 1 & 0 \\ 0 & 0 & 0 & 1 \\ 0 & \frac{ad}{E} & \frac{-Bb}{E} & 0 \\ & \frac{bd}{E} & \frac{-Bc}{E} & 0 \end{bmatrix} \begin{bmatrix} \alpha \\ \theta \\ \dot{\alpha} \\ \dot{\theta} \end{bmatrix} + \begin{bmatrix} 0 \\ 0 \\ \frac{b}{E} \\ \frac{c}{E} \end{bmatrix} T \tag{5.57}$$

$$y = \begin{bmatrix} 1 & 0 & 0 & 0 \\ 0 & 1 & 0 & 0 \end{bmatrix} \begin{bmatrix} \alpha \\ \theta \\ \dot{\alpha} \\ \dot{\theta} \end{bmatrix} \tag{5.58}$$

General state space form is

$$\dot{x} = \mathbf{A}x + \mathbf{B}u \tag{5.59}$$

$$y = \mathbf{C}x + \mathbf{D}u \tag{5.60}$$

Then, for the rotary inverted pendulum system, when the parameters are inserted, below matrices are obtained.

$$\mathbf{A} = \begin{bmatrix} 0 & 0 & 1 & 0 \\ 0 & 0 & 0 & 1 \\ 0 & 0.158 & -0.040 & 0 \\ 0 & 184.001 & -0.016 & 0 \end{bmatrix} \tag{5.61}$$

$$\mathbf{B} = \begin{bmatrix} 0 \\ 0 \\ 9.999 \\ 4.031 \end{bmatrix} \mathbf{C} = \begin{bmatrix} 1 & 0 & 0 & 0 \\ 0 & 1 & 0 & 0 \end{bmatrix} \tag{5.62}$$

$$\mathbf{D} = 0 \tag{5.63}$$

Controllability of the System In this part, controllability of the system is examined. Controllability matrix is constructed and it is shown that it is a full rank matrix.

$$\textbf{cont} = \begin{bmatrix} \mathbf{B} & \mathbf{AB} & \mathbf{A}^2\mathbf{B} & \mathbf{A}^3\mathbf{B} \end{bmatrix} \tag{5.64}$$

$$\textbf{cont} = \begin{bmatrix} 0 & 9.999 & -0.399 & 0.654 \\ 0 & 4.031 & -0.161 & 741.676 \\ 9.999 & -0.399 & 0.6535 & -0.0516 \\ 4.031 & -161 & 741.676 & -29.674 \end{bmatrix} \tag{5.65}$$

$$rank(\textbf{cont}) = 4 \tag{5.66}$$

State Space Model and Controllability in Discrete Domain In this part, due to the nature of the PW modulated actuator, discrete model is constructed and its controllability is examined.

Discrete model is constructed from continuous time state space form:

$$\mathbf{x}((k+1)T) = \mathbf{A}_z(T)\mathbf{x}(kT) + \mathbf{B}_z u(kT) \tag{5.67}$$

Where;

$$\mathbf{A}_z(T) = e^{\mathbf{A}T} \tag{5.68}$$

$$\mathbf{B}_z(T) = \left(\int_0^T e^{\mathbf{A}T} dt \right) \mathbf{B} \tag{5.69}$$

Firstly, the state space equation is converted to discrete domain for 2 Hz PWM frequency, which corresponds to 0.5 seconds sampling period. For this case, state and controllability matrix is given in Equations 5.70, 5.71 and 5.72. Since the matrix is not a full rank matrix, the system is not controllable for a selected sampling period.

$$\mathbf{A}_z = \begin{bmatrix} 1 & 0.09 & 0.5 & 0.01 \\ 0 & 20.28 & 0 & 2.74 \\ 0 & 0.74 & 1 & 0.1 \\ 0 & 149.97 & 0 & 20.28 \end{bmatrix} \tag{5.70}$$

$$\mathbf{B}_z = \begin{bmatrix} 0.18 \\ 0.6 \\ 0.73 \\ 4.67 \end{bmatrix} \tag{5.71}$$

$$\mathbf{cont} = \begin{bmatrix} 0 & 0 & 0 & 0.0002 \\ 0 & 0 & 0 & 0.5024 \\ 0 & 0 & 0 & 0.0041 \\ 0 & 0 & 0.00076 & 9.6384 \end{bmatrix} \tag{5.72}$$

After that, the PWM frequency selected as 20 Hz and the discrete domain state space form is constructed. For this case, controllability matrix is full rank. It is resulted that as PWM frequency lowered controllability is lost for the system.

Full State Feedback Controller In this part, a linear control method, full state feedback controller is designed. All states are assumed as measurable. Block diagram of the full state feedback controller is given in Figure 5.15 [14]. In this figure,

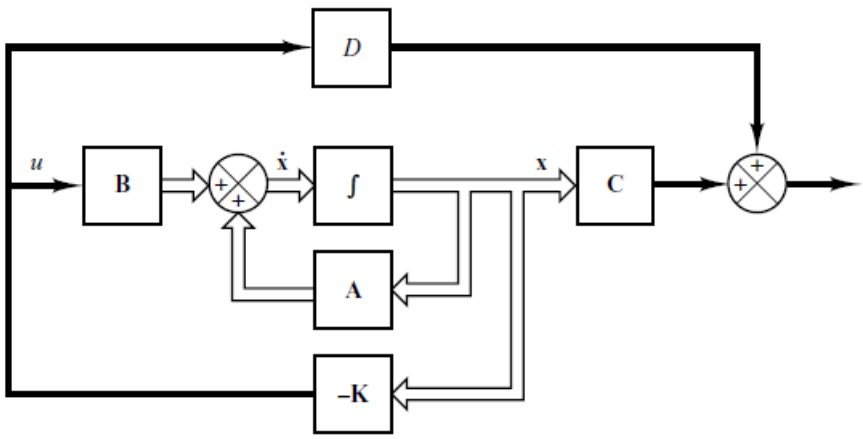

Figure 5.15: Full State Feedback Block Diagram[14]

K is the state feedback gain matrix. Mathematical expression of the overall closed loop system is

$$\dot{x} = (\mathbf{A} - \mathbf{BK})x \tag{5.73}$$

The term in the parenthesis in the above equation determines the characteristics of the closed loop system. The eigenvalues of this term must be equal to desired pole locations. Calculation of matrix **K** to satisfy the eigenvalues requirement is done by Ackermann's formula that given as Equations 5.74 and 5.75.

$$\mathbf{K} = \begin{bmatrix} 0 & 0 & 0 & 1 \end{bmatrix} \begin{bmatrix} \mathbf{B} & \mathbf{AB} & \mathbf{A}^2\mathbf{B} & \mathbf{A}^3\mathbf{B} \end{bmatrix}^{-1} \phi(\mathbf{A}) \tag{5.74}$$

$\phi(\mathbf{A})$ is given below. In the below equation α_1, α_2, α_3 and α_4 are the coefficients of the desired characteristic equations.

$$\phi(\mathbf{A}) = \mathbf{A}^4 + \alpha_1\mathbf{A}^3 + \alpha_2\mathbf{A}^2 + \alpha_3\mathbf{A} + \alpha_4\mathbf{I} \tag{5.75}$$

Full State Feedback Controller in Discrete Domain State feedback controller is designed in z domain also. Closed loop state space form of the system is given as Equation 5.76. State feedback gain matrix is calculated by using Ackermann's formula those given as Equations 5.74 and 5.75.

$$\mathbf{x}(k+1) = (\mathbf{A}_z - \mathbf{B}_z\mathbf{K})\mathbf{x}(k) \tag{5.76}$$

5.3.3.3 Switching Controller

Switching controller switches the controller scheme between the swing-up and the balancing controllers. As stated in the balancing controller section, the equation of motion of the rotary inverted pendulum is assumed as linear around the equilibrium point. Switching controller decides which controller is to be used according to the pendulum position.

The switching controller switches the controller to the balancing mode when the absolute value of the pendulum is smaller than 10 degrees and it switches the controller to the swing-up mode for higher angles.

5.3.4 Simulation Results

In this section, simulation results of the inverted pendulum are presented. To be able to observe the swing-up motion and effects of the nonlinearities, the nonlinear inverted pendulum model is constructed as seen from Figure 5.16. Simulations are done with different PWM frequencies and controller gains.

Angular position simulation is run for 10 Hz PWM frequency and discrete analysis. The controller was unable to catch and balance the inverted pendulum at the upright position. Another simulation was run with 20 Hz PWM frequency and continuous analysis. This controller was also unable to catch and balance the inverted pendulum at the upright position.

Figure 5.17 shows the angular position of the pendulum for 20 Hz PWM frequency and gains calculated by the discrete controller. According to the figure, it takes about 8 seconds to swing-up the pendulum to the up-right position. Simulation result is satisfying with discrete analysis and high frequency PWM.

Figure 5.18 shos thrust ouptut which is the control input during inverted pendulum simulation.

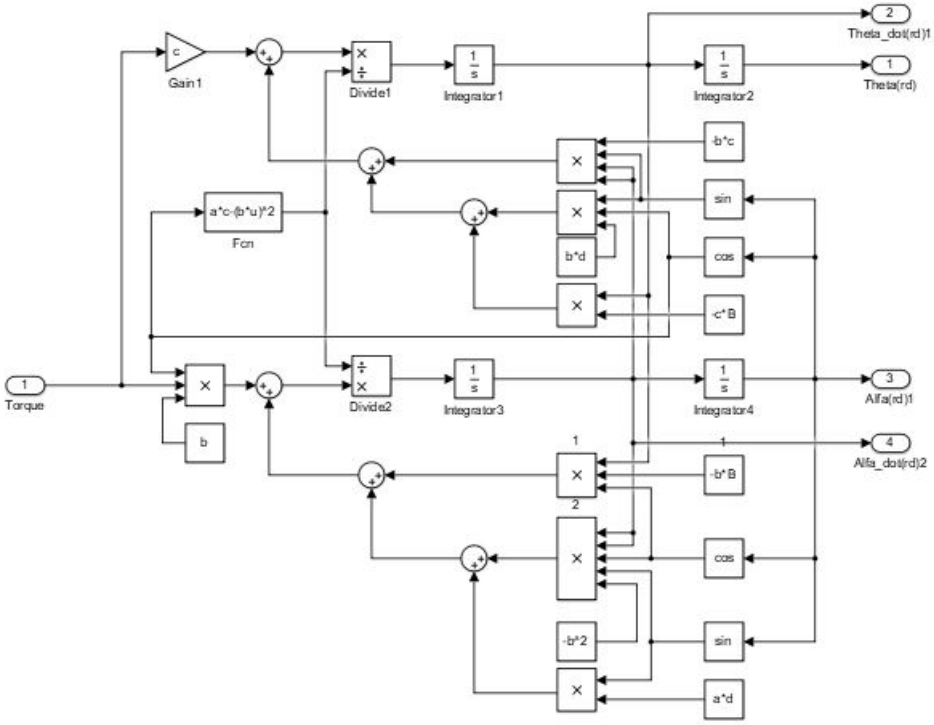

Figure 5.16: Nonlinear Pendulum Model

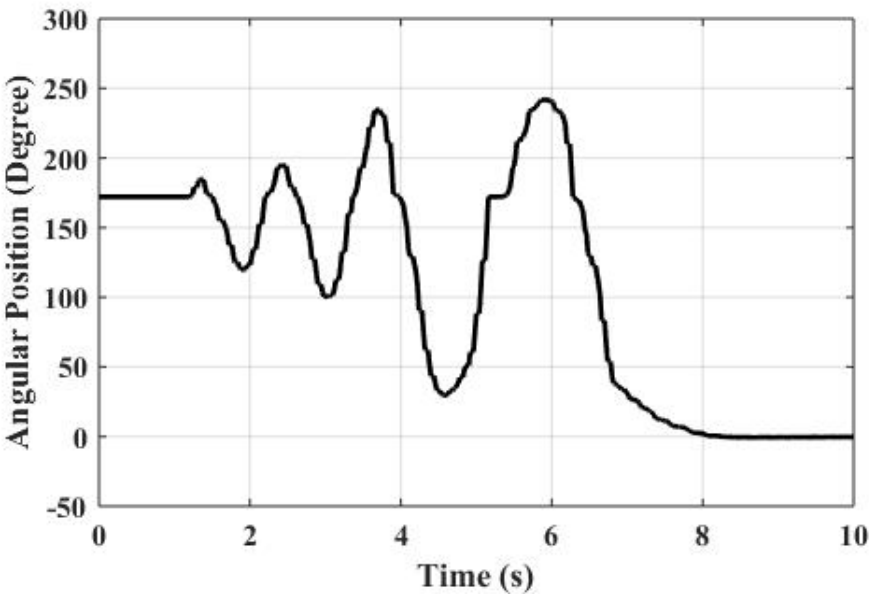

Figure 5.17: Inverted Pendulum Simulation Result

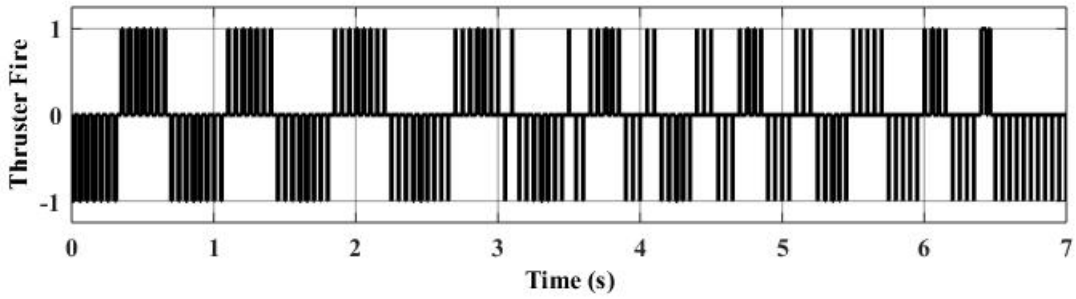

Figure 5.18: Inverted Pendulum Simulation - Thrust Output

5.4 Closure

In this chapter, controller design and simulation results are presented for the single axis angle platform and the rotary inverted pendulum applications.

Dynamical model is constructed for both applications. Due to the sample and hold dynamics of the PWM application, models are discretized for the selected PWM frequencies. Controller gains are calculated by both continous and discrete analysis and the results are compared.

Regarding the single axis platform, without modulation and the modulation with continuous and discrete controller are compared. It is shown that for low system bandwidth and high PWM frequency cases, the results are comparable. However, as the PWM frequency and the system bandwidths get closer, effects of the bang-bang actuator and the sample-hold effect gets higher. For this case, the discrete controller with modulation gave satisfying results. Rate limiter also proposed for obtaining high performance for small angles and good linear control performance for higher angle commands.

For the inverted pendulum application, it is shown that controllability is lost for low frequency PWM application. Simulation results show that high frequency PWM with discrete analysis is required for on/off under actuated, non-linear and naturally unstable system.

CHAPTER 6

RESULTS OF THE EXPERIMENTS

6.1 Introduction

In this chapter, results of the experiment related to the single axis and the rotary inverted pendulum are presented. Firstly, the details of the experimental test setup are presented. Then, the results of the single axis and the inverted pendulum experiments are discussed. Performance of the controllers are discussed. Discrepancies between the simulation and the experimentation results are elaborated. Finally, this chapter is concluded with closing comments.

6.2 Experimental Test Setup

In this section, details of the experimental test setups are presented. For the single axis and the inverted pendulum test setups almost the same components are used. The only difference is a rotary encoder mounted on the single axis platform for the inverted pendulum test setup. The pendulum is attached to the rotary encoder. Test setup parts can be separated as the parts related to structural, pneumatic, data acquisition and control duties. These parts are listed in Table 6.1.

Structural part of the test setup is composed of a base part and a rod attached to the base part by a bearing. Base part, rod and other mechanical parts are manufactured using a 3D printer. The bearing provides unlimited and low frictional rotational motion.

Pneumatic part of the test setup is composed of pressure regulator, two on/off solenoid

Table 6.1: Experimental Test Setup Devices

Devices	
Pressure Regulator	Norgren Olympian Plus
Solenoid Vale	MHJ10-S-2,5-QS-6-hf
Rotating Pneumatic Fitting	QSML-G1/8-4
Real Time Target Machine	Speedgoat Performance
FPGA	IO331 FPGA Module
Rotary Incremental Encoder	Yumo-E6B2-CWZ3E-1024
Slip Ring	22 mm 240V@2A-24A

valves, pipes and rotating pneumatic fitting. Pressured gas is provided to the pressure regulator. Pressure regulator ensures constant pressure for the valves. Pressure regulator is placed at the outside of the test setup, but the valves are placed on the rotating platform. To provide air supply from the regulator to the valves without preventing rotational motion, low friction rotating pneumatic fitting is used.

Data acquisition, control and signal/power routing part of the test setup are composed of real time target machine, two incremental rotary type encoders, slip ring and DC power supply. Rotary encoders are the sensors of the control loop and they measure the rotational positions of the rod and the pendulum. Real time target machine takes encoder data, contains control loop and creates control commands for the valve. Signals and power are delivered to the valve and the encoders using rotational slip ring. In test setup, by using pneumatic rotating joint and slip ring, unlimited and low frictional rotational motion is provided.

Figures 6.1 and 6.2 show photographs of the single axis and the rotary inverted pendulum test setups, respectively. Figure 6.3 shows the block diagram of the test setup. Details of some of the critical components of the test setups are listed below.

6.2.1 Pressure Regulator

Figure 6.4 shows the pressure regulator used in the test setup. 10 to 12 Bar pressurized air is supplied to the regulator and the regulator output pressure can be arranged between 2 to 8 bar manually.

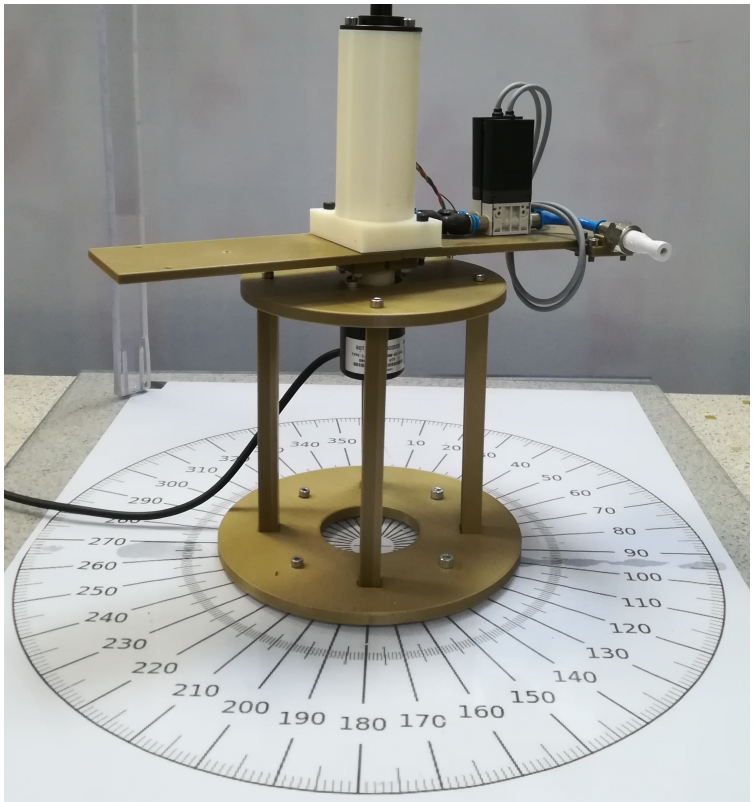

Figure 6.1: Single Axis Test Platform

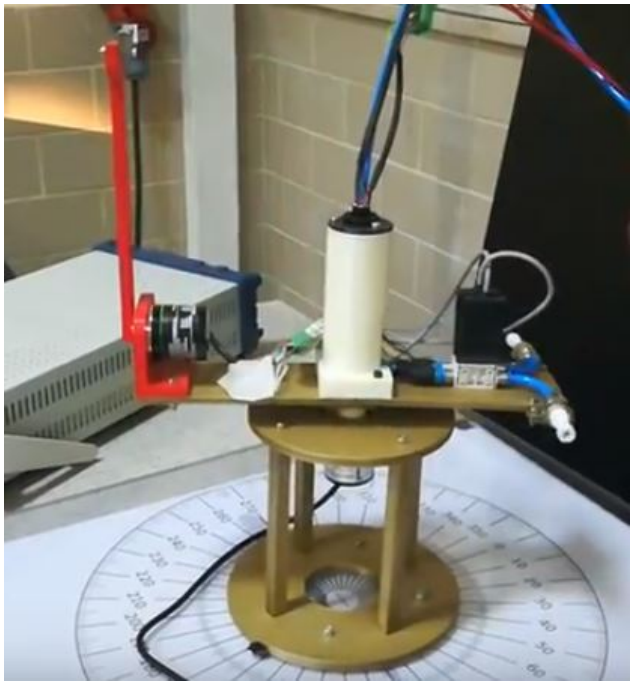

Figure 6.2: Rotary Inverted Pendulum Test Setup

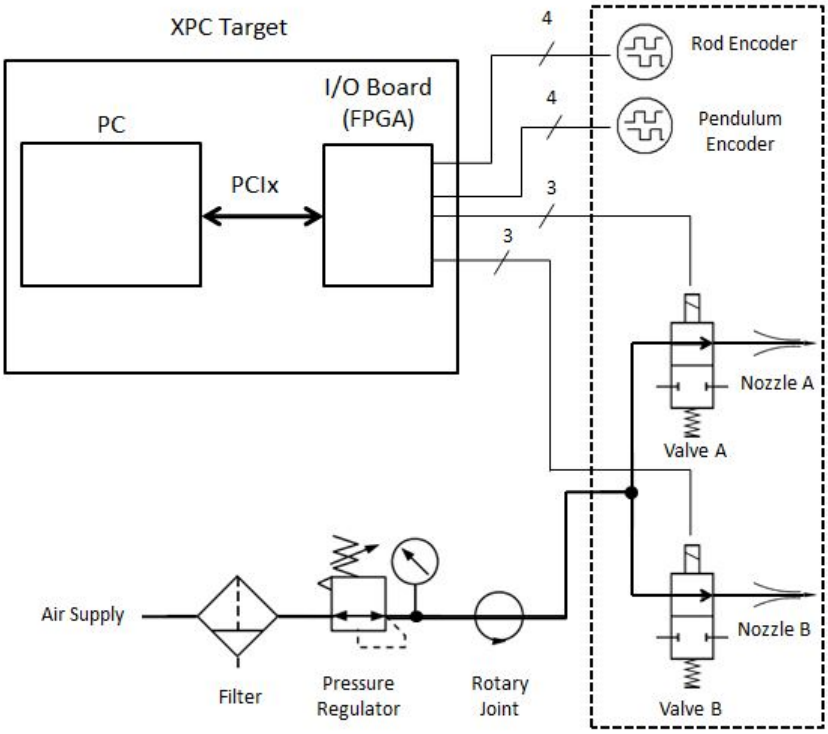

Figure 6.3: General Block Diagram of the Test Setup

Figure 6.4: Pressure Regulator

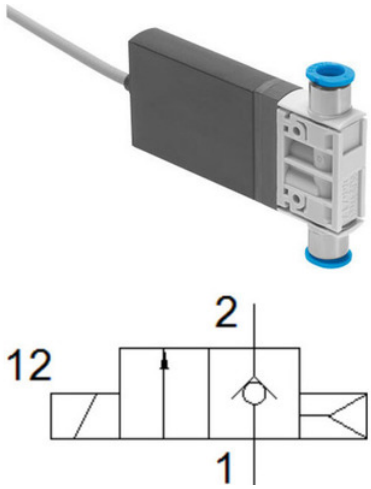

Figure 6.5: On/off Solenoid Valve

6.2.2 Solenoid Valve

In this test setup, solenoid valve, shown as Figure 6.5, is a two way normally closed on/off valve. Characterization of the valve is given in Chapter 3. Solenoid valve used in this work comes with integrated driver that ensure usage without need of external driver. For the valves which does not have any integrated driver a solenoid driver or a brushed motor driver can be used to drive the solenoid. As an example of a driver functional diagram of a solenoid drive DRV120 is given as Figure 6.6.

6.2.3 Rotating Pneumatic Fitting

Pneumatic fitting, shown in Figure 6.7, ensures limitless and low frictional rotational motion while delivering constant pressure air to the valves. By using this fitting, the need for gas tank and pressure regulator on the test setup is eliminated and the test setup becomes way more lighter, cheaper and easier to produce.

6.2.4 Real Time Target Machine

Real time target machine used in the test setup is 'Speedgoat Performance Real Time Target Machine' shown in Figure 6.8. The target is used for running the control loop and generating pulse commands for on/off valves. IO/331 FPGA module (Figure 6.9),

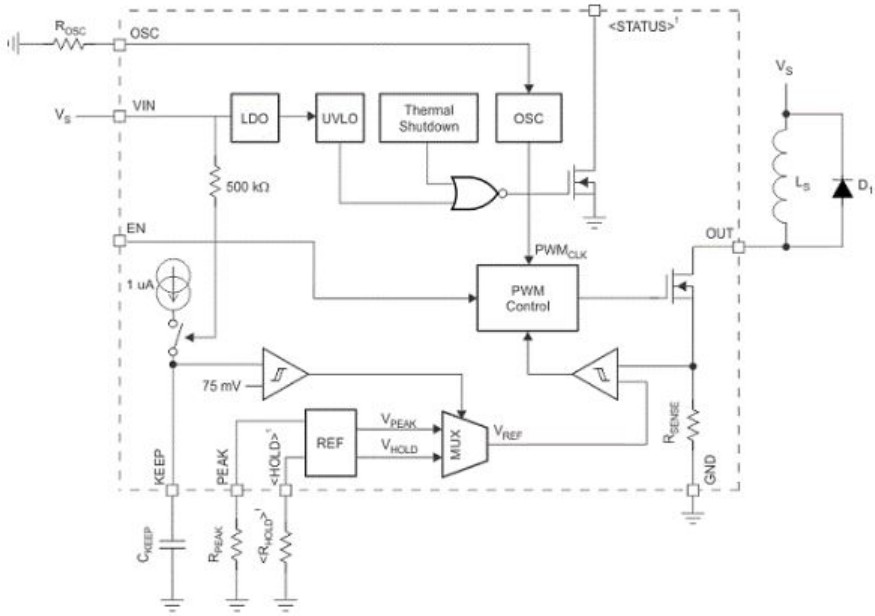

Figure 6.6: Functional Diagram of the Solenoid Driver DRV120

Figure 6.7: Rotating Pneumatic Fitting

Figure 6.8: Real Time Target Machine

Figure 6.9: IO/331 FPGA Module

mounted on the target, is used for the quadrature encoder decoding of rotary encoders and generating PWM commands.

Main advantage of using this target machine is that the drivers are provided for Matlab/Simulink. By using these drivers, the controller scheme is constructed on Matlab/Simulink and directly used on the target by making only small arrangements.

6.2.5 Rotary Incremental Encoder

In test setup, two rotary incremental encoders (Figure 6.10 are used. The one used for rod angle measurement generates 400 pulse for one revolution and the one used for the pendulum angle measurement generates 1024 pulse per revolution. Encoded data

Figure 6.10: Rotary Incremental Encoder

Figure 6.11: Slip Ring

are decoded in quadrature mode by using quadrature encoder decoding module of IO/331 module. By using quadrature decoding, the obtained resolution is 4 times of the generated pulse per revolution. Thus, the rod angle is measured with 1600 cycles per revolution and the pendulum angle is measured with 4096 cycles per revolution resolution.

6.2.6 Slip Ring

Slip ring (Figure 6.11) is used for transmitting signal and power between the devices on the rotating platform (encoder for pendulum and valves) and other devices that are not placed on the rotating platform (power supply and real time target machine). By using slip ring, spring and damping effects are minimized and unlimited rotation is provided.

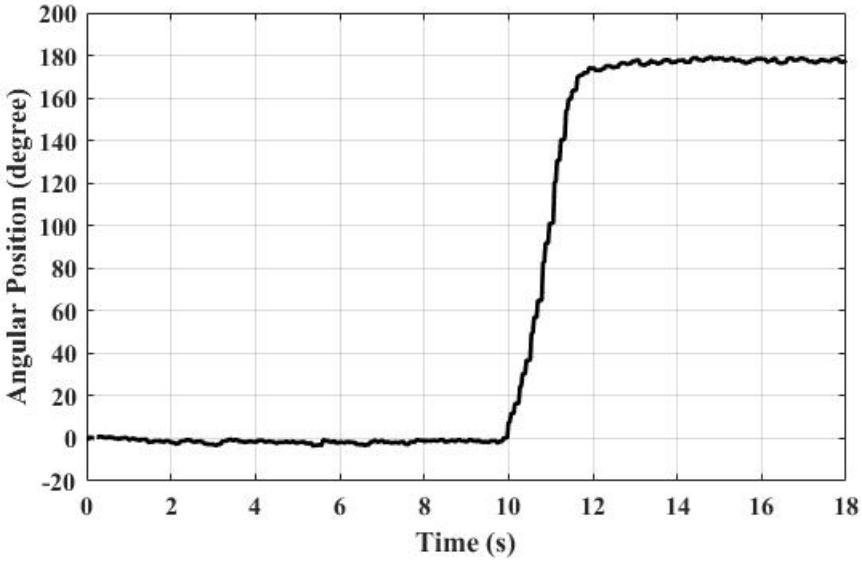

Figure 6.12: Angular Position of the Rotational Platform

6.3 Single Axis Experiment Results

In this section, results of the single axis control of a rotational platform experiment are discussed. Firstly, graphics related to experiment results are presented. Then, the results are compared with the simulation results provided in Chapter 5. Finally, discrepancies between the model and test setup are examined.

Figure 5.12 shows the angular position of the rotational platform during the single axis motion. For particular experiment, a 180 degree angle command has applied on the system. According to the figure, it takes two seconds for the closed loop system to reach to the reference position. System does not have any overshoot and it has about 1 degree of steady state error.

When compared with Section 5.12, in which the simulation results for the same case are provided, the simulation and test results are comparable. Rise times are slightly different for both cases. The reasons of the difference are the spring and damping effects of the rotary pneumatic joint, piping and slip ring. Figure 6.13 shows the thruster output during single axis motion.

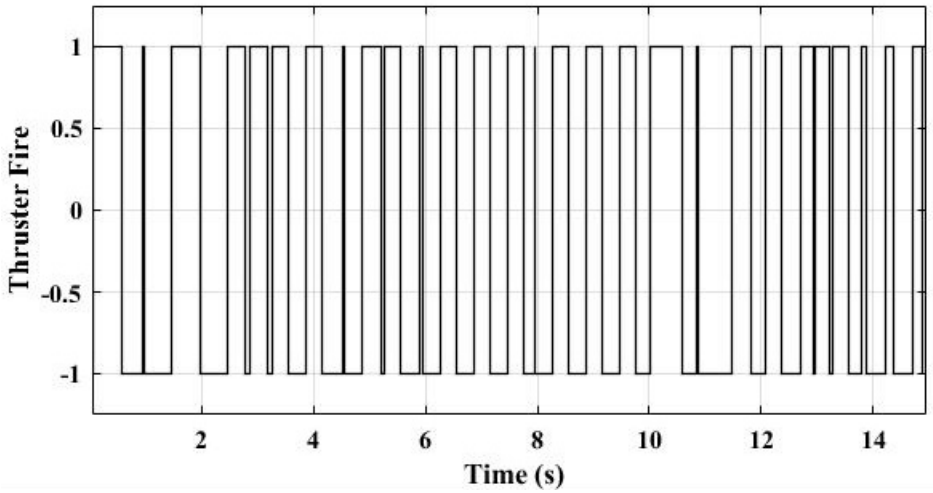

Figure 6.13: Thruster Fire during Single Axis Motion

6.4 Inverted Pendulum Experiment Results

In this section, results of the rotary inverted pendulum experimentation are presented. Firstly, graphics related to the experiment results are given. Controller performance and the discrepancies between the model and the experiment results are discussed.

Figure 6.14 shows the angular position of the pendulum during the swing-up and the balancing motions. According to the figure, it takes 4 swings for the pendulum to reach to the unstable equilibrium position. Balancing controller does not have any overshoot and it has no steady state error as desired. Figure 6.15 shows the thruster output during the motion.

The inverted pendulum test result is also comparable with the simulation results provided in Section 5.17. Similar to the single axis application, the reason of the discrepancies between the model and the simulation are considered to be the piping and the slip ring.

6.5 Closure

In this chapter, experimental test setups are introduced and the test results are provided. Results are compared with the simulations. Simulation and experiment results were close, however there were discrepancies. Especially for single axis angle con-

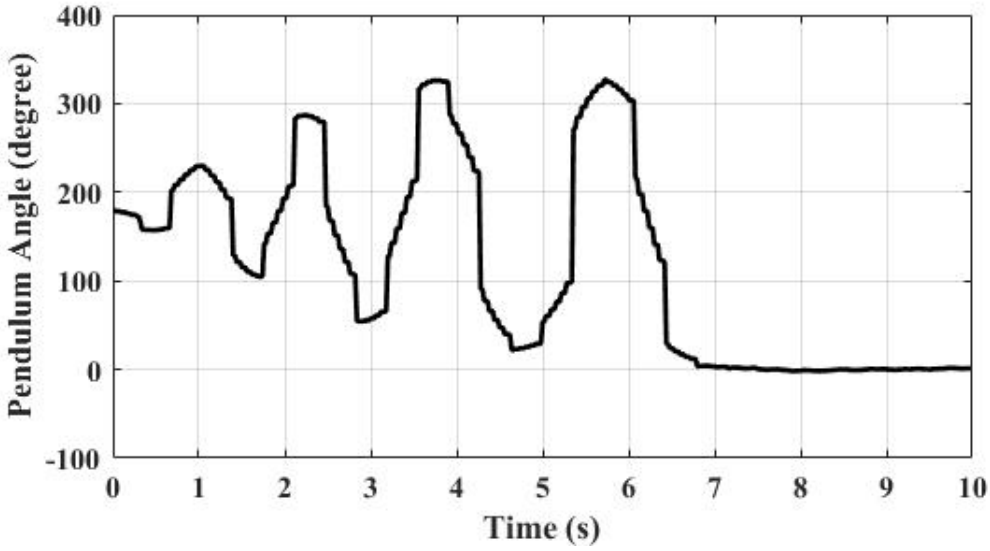

Figure 6.14: Angular Position of Pendulum

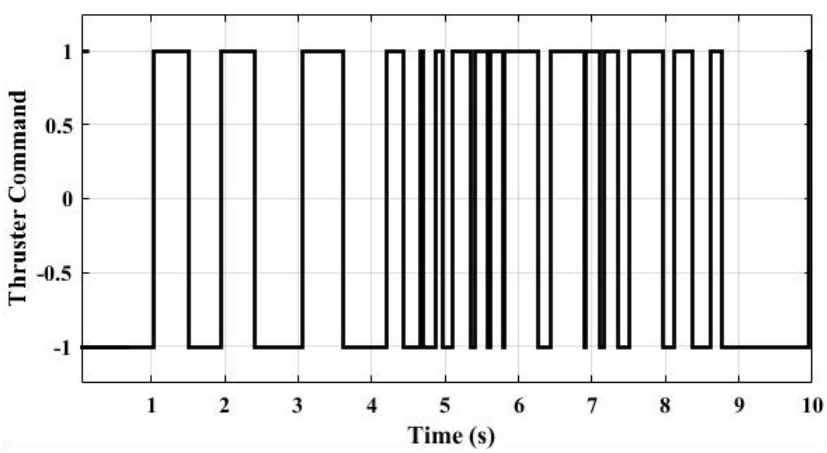

Figure 6.15: Thruster Fire During Pendulum Motion

troller, which is a simplified version of attitude control of a spacecraft, space like environment is required. Due to the restrictions, it is highly challenging to achieve friction-less environments. As a result, discrepancies are observed for both the single axis angle control application and the rotary inverted pendulum experimentation.

CHAPTER 7

CONCLUSIONS AND FUTURE WORKS

7.1 Conclusions

In this work, a PWM-based thrust control method for cold gas thruster system is proposed. Firstly, model of an on/off type of solenoid valve is constructed and experimentally validated. Then, a method for PWM frequency selection is proposed. Lastly, PWM actuated cold gas thrusters are used for the single axis and the inverted pendulum applications.

Pulse width modulator is used to be able to obtain quasi-linear thrust output. While selecting the PWM frequency, switching restrictions of an on/off valve is also taken into account. Characterization of the thruster valve is required to obtain switching restrictions. Firstly, mathematical model of a solenoid valve is constructed. It is observed from the mathematical model that the solenoid plunger movement instants overlap with local minima and maxima points of the solenoid current. This phenomenon is used to obtain the opening and closing time intervals of the valve by current experimentation. Discrepancies are observed between the model and the experiment results. It is commented that the major discrepancy comes from the voltage rising time for the real system, and the model is updated accordingly. Since the rise time of the input voltage is related with the used voltage source, micro-controller and other electrical connections, making the test with close to the real application version will result with better accuracy.

After the valve characterization, PWM frequency selection method is proposed. It is shown that using higher frequency PWM results with high minimum and maximum

duty value limits. This results with high controller dead-band and low quasi-linear working range for the linear controller. However, it is also shown that the bandwidth of the actuator gets lower via decreasing the PWM frequency. Hence, the actuator cannot track high frequency thrust commands and it reduces overall system bandwidth. In this work, the relation between the actuator dead-band and the PWM frequency is formalized. By using the given formulation for the required duty value limits, the required maximum PWM frequency can be calculated. Obtained equations can also be used to calculate the duty value limits for the selected PWM frequency.

PW modulated thruster valve model is used as an actuator for the single axis angle control and the inverted pendulum application. Relationship between the system bandwidth and the PWM frequency is examined for both of the systems. Affect of the sample and hold effect due to the PW modulation is examined for controllability and system performance. Discrete analysis is carried out for better dynamic performance.

Single axis simulations are carried out for different cases. From these simulations different conclusions are obtained. First, for low frequency system bandwidth case, using actuator as bang-bang gives good linear response. However, number of thruster fire required for the operation is much higher than the modulated cases. As thrust fire increases electrical power, propellant and valve wear also increases. This is undesired as the same performance can be obtained with less number of thruster firings. Although for low frequency system bandwidth, the un-modulated position response result is satisfying. However, the linear controller results with undesired response for high frequency system bandwidth. Simulations are also showed that calculating controller gains by continuous analysis may result with undesired response for modulated case. The obtained response gets worse as the system bandwidth and PWM frequency get closer as expected. Controller gains calculated by discrete analysis resulted with good results with PW modulated actuator. With this configuration, the system can track required steps and sinusoidal commands. For this configuration, the rate limiter is also proposed for high angular command to prevent saturation. Thus, required bandwidth is accomplished for small angle commands and saturation and overshoot are avoided for high angle commands.

PWM modulated on/off actuator with linear controller is tried with relatively hard sys-

tem, which is a rotary inverted pendulum. Another challenge ,on/off actuator dynamics, is added to nonlinear, under actuated and naturally unstable system. In addition to that, on/off cold gas thruster actuator is used for the first time with the inverted pendulum application. For this application, it is observed that as sampling period increases, controllability of the system is lost. Thus, it is evaluated that for controllability PWM frequency must be greater than some value and as PWM frequency increases it is easier to control the system. Simulation results also showed that continuous analysis is not enough for this system and discrete analysis is required.

Single axis angle control and inverted pendulum application are tested on laboratory level test setups. It was challenging to create space like environments. Although slip ring and rotary pneumatic joint are used for creating low frictional rotational motion, spring and damping effect of the piping and the pneumatic rotary joint were pretty effective. Under these circumstances designed modulator and controllers are tried on both the single axis angular position and the rotary inverted pendulum control test setups. The performance of the controllers were satisfying. However, discrepancies are observed between the model and the experimentation results. It is evaluated that the major cause of the discrepancies are friction and spring effects.

The best use of the proposed controller schemes in this work might be the multi-input multi-output (especially under-actuated ones) on/off thruster actuated spacecraft attitude control problems. For these kind of problems to be able to control all states simultaneously, independent torques are required for three axis. For under actuated system to obtain independent torques for every axis combination of quasi-linear output of thruster is required. If the system is completely state controllable, the controller for this system can be designed by linear state space analysis. Thus, for this case required quasi-linear thrust can be obtained by proper PW modulator and sampler dynamics of the modulator can be taken into account by discrete analysis. The required fast response can be obtained for every angular position.

Inverted pendulum applications are accomplished with different types of actuators using different configurations. This work extends the topic by using another type of actuator with different dynamics. The used actuator adds system another challenge, which is low frequency on/off actuator dynamics.

7.2 Future Works

Proposed design method can be used for attitude control experimentation. Performance of the overall controller may be improved with different types of thruster placement configurations.

REFERENCES

[1] A. Anis, "Cold gas propulsion system-an ideal choice for remote sensing small satellites," in *Remote sensing-advanced techniques and platforms*, IntechOpen, 2012.

[2] R. Vazquez, F. Gavilan, and E. F. Camacho, "Trajectory planning for spacecraft rendezvous with on/off thrusters," in *IFAC World Congress*, vol. 18, pp. 8473–8478, Citeseer, 2011.

[3] T. Sakamoto and N. Hori, "New pwm schemes based on the principle of equivalent areas," in *IEEE International Symposium on Industrial Electronics, L'Aquila, Italy*, pp. 505–510, 2002.

[4] D. J. Zimpfer, L. S. Shieh, and J. W. Sunkel, "Digitally redesigned pulse-width modulation spacecraft control," *Journal of guidance, control, and dynamics*, vol. 21, no. 4, pp. 529–534, 1998.

[5] F. Bernelli-Zazzera and P. Mantegazza, "Pulse-width equivalent to pulse-amplitude discrete control of linearsystems," *Journal of guidance, control, and dynamics*, vol. 15, no. 2, pp. 461–467, 1992.

[6] J. Alcorn, H. Schaub, and S. Piggott, "Steady-state attitude and control effort sensitivity analysis of discretized thruster implementations," *Journal of Spacecraft and Rockets*, vol. 54, no. 5, pp. 1161–1169, 2017.

[7] G. Howells and M. Gillham, "Attitude control of small probes for de-orbit, descent and surface impact on airless bodies using a single pwm thruster," 2017.

[8] A. Mazinan, M. Pasand, and B. Soltani, "Full quaternion based finite-time cascade attitude control approach via pulse modulation synthesis for a spacecraft," *ISA transactions*, vol. 58, pp. 567–585, 2015.

[9] T. Suzuki, T. Ueno, and N. Hori, "Experimental verification of pea-based pwm control using on-off type air-jet thrusters," in *Proceedings of the International Conference on Information and Automation*, pp. 1–6, 2005.

[10] S. W. Jeon and S. Jung, "Hardware-in-the-loop simulation for the reaction control system using pwm-based limit cycle analysis," *IEEE Transactions on control systems technology*, vol. 20, no. 2, pp. 538–545, 2012.

[11] J. Bals and K. Kienitz, "A comprehensive approach to pulse modulation for attitude control with thrusters subject to switching restrictions,"

[12] M. Taghizadeh, A. Ghaffari, and F. Najafi, "Modeling and identification of a solenoid valve for pwm control applications," *Comptes Rendus Mecanique*, vol. 337, no. 3, pp. 131–140, 2009.

[13] E. E. Topçu, İ. Yüksel, and Z. Kamış, "Development of electro-pneumatic fast switching valve and investigation of its characteristics," *Mechatronics*, vol. 16, no. 6, pp. 365–378, 2006.

[14] K. Ogata and Y. Yang, *Modern control engineering*, vol. 4. Prentice-Hall, 2002.

[15] K. Ogata *et al.*, *Discrete-time control systems*, vol. 2. Prentice Hall Englewood Cliffs, NJ, 1995.

[16] L. Jasper and H. Schaub, "Tethered towing using open-loop input-shaping and discrete thrust levels," *Acta Astronautica*, vol. 105, no. 1, pp. 373–384, 2014.

[17] J.-P. Thiran, "Recursive digital filters with maximally flat group delay," *IEEE Transactions on Circuit Theory*, vol. 18, no. 6, pp. 659–664, 1971.

[18] T. I. Laakso, V. Valimaki, M. Karjalainen, and U. K. Laine, "Splitting the unit delay [fir/all pass filters design]," *IEEE Signal Processing Magazine*, vol. 13, no. 1, pp. 30–60, 1996.

[19] T. Matsumoto, K. Kita, R. Suzuki, A. Oosedo, K. Go, Y. Hoshino, A. Konno, and M. Uchiyama, "A hovering control strategy for a tail-sitter vtol uav that increases stability against large disturbance," in *2010 IEEE international conference on robotics and automation*, pp. 54–59, IEEE, 2010.

[20] R. Tekin, Ö. Atesoglu, and K. Leblebicioglu, "Modeling and vertical launch analysis of an aero-and thrust vector controlled surface to air missile," in *AIAA Atmospheric Flight Mechanics Conference*, p. 7639, 2010.

[21] K. Sreekumar and A. Ramchandani, "Launch stabilisation system for vertical launch of a missile," *Defence Science Journal*, vol. 55, no. 3, pp. 223–230, 2005.

[22] B. Andrievsky, "Global stabilization of the unstable reaction-wheel pendulum," *Automation and Remote Control*, vol. 72, no. 9, p. 1981, 2011.

[23] J. M. Adler, M. S. Lee, and J. D. Saugen, "Adaptive control of propellant slosh for launch vehicles," in *Sensors and sensor integration*, vol. 1480, pp. 11–23, International Society for Optics and Photonics, 1991.

[24] B. Bandyopadhyay, S. Kurode, and P. Gandhi, "Sliding mode control for slosh-free motion-a class of underactuated system," *International Journal of Advanced Mechatronic Systems*, vol. 1, no. 3, pp. 203–213, 2009.

[25] B. Bandyopadhyay, P. Gandhi, and S. Kurode, "Sliding mode observer based sliding mode controller for slosh-free motion through pid scheme," *IEEE Transactions on Industrial Electronics*, vol. 56, no. 9, pp. 3432–3442, 2009.

[26] S. Cho, M. McClamroch, and M. Reyhanoglu, "Feedback control of a space vehicle with unactuated fuel slosh dynamics," in *AIAA Guidance, Navigation, and Control Conference and Exhibit*, p. 4046, 2000.

[27] J. R. Hervas and M. Reyhanoglu, "Thrust-vector control of a three-axis stabilized upper-stage rocket with fuel slosh dynamics," *Acta Astronautica*, vol. 98, pp. 120–127, 2014.

[28] E. V. Kumar and J. Jerome, "Robust lqr controller design for stabilizing and trajectory tracking of inverted pendulum," *Procedia Engineering*, vol. 64, pp. 169–178, 2013.

[29] C.-S. Chen and W.-L. Chen, "Robust adaptive sliding-mode control using fuzzy modeling for an inverted-pendulum system," *IEEE Transactions on Industrial Electronics*, vol. 45, no. 2, pp. 297–306, 1998.

[30] R.-J. Wai and L.-J. Chang, "Adaptive stabilizing and tracking control for a nonlinear inverted-pendulum system via sliding-mode technique," *IEEE Transactions on Industrial Electronics*, vol. 53, no. 2, pp. 674–692, 2006.

[31] M. I. El-Hawwary, A.-L. Elshafei, H. M. Emara, and H. A. A. Fattah, "Adaptive fuzzy control of the inverted pendulum problem," *IEEE Transactions on Control Systems Technology*, vol. 14, no. 6, pp. 1135–1144, 2006.

[32] K. Furuta, M. Yamakita, and S. Kobayashi, "Swing up control of inverted pendulum," in *Proceedings IECON'91: 1991 International Conference on Industrial Electronics, Control and Instrumentation*, pp. 2193–2198, IEEE, 1991.

[33] J. Wen, Y. Shi, and X. Lu, "Stabilizing a rotary inverted pendulum based on logarithmic lyapunov function," *Journal of Control Science and Engineering*, vol. 2017, 2017.

[34] X. Yang and X. Zheng, "Swing-up and stabilization control design for an underactuated rotary inverted pendulum system: theory and experiments," *IEEE Transactions on Industrial Electronics*, vol. 65, no. 9, pp. 7229–7238, 2018.

[35] G. Sainzaya, F.-N. Yu, T.-L. Hsieh, and C.-Y. Yang, "Lqr control with refined pid to balance rotary inverted pendulum with time-varying uncertainty," in *2017 International Conference on Fuzzy Theory and Its Applications (iFUZZY)*, pp. 1–6, IEEE, 2017.

[36] K. Srinivas and L. Behera, "Swing-up control strategies for a reaction wheel pendulum," *International Journal of Systems Science*, vol. 39, no. 12, pp. 1165–1177, 2008.

[37] M. W. Spong, P. Corke, and R. Lozano, "Nonlinear control of the reaction wheel pendulum," *Automatica*, vol. 37, no. 11, pp. 1845–1851, 2001.

[38] B. Bapiraju, K. Srinivas, P. P. Kumar, and L. Behera, "On balancing control strategies for a reaction wheel pendulum," in *Proceedings of the IEEE INDICON 2004. First India Annual Conference, 2004.*, pp. 199–204, IEEE, 2004.

[39] J. Petric and Z. Situm, "Inverted pendulum driven by pneumatics," *International Journal of Engineering Education*, vol. 19, no. 4, pp. 597–602, 2003.

[40] T. Žilić, D. Pavković, and D. Zorc, "Modeling and control of a pneumatically actuated inverted pendulum," *ISA transactions*, vol. 48, no. 3, pp. 327–335, 2009.

[41] Z. Shenghao and S. Jinchun, "Intelligent predictive fuzzy control for pneumatic inverted pendulum," in *2011 6th IEEE Conference on Industrial Electronics and Applications*, pp. 968–972, IEEE, 2011.

[42] W. N. White and R. C. Fales, "Control of a double inverted pendulum with hydraulic actuation: A case study," in *Proceedings of the 1999 American Control Conference (Cat. No. 99CH36251)*, vol. 1, pp. 495–499, IEEE, 1999.

[43] A. Makled, M. AL-Sanabawy, and M. Bakr, "Theoretical and experimental evaluation of cold gas system components," in *13 th International Conference of Aerospace Sciences & Aviation Technology, ASAT–13*, p. 23, 2009.

[44] J. R. Brauer, *Magnetic actuators and sensors*. John Wiley & Sons, 2006.

[45] E. E. Topçu, İ. Yüksel, and Z. Kamış, "Development of electro-pneumatic fast switching valve and investigation of its characteristics," *Mechatronics*, vol. 16, no. 6, pp. 365–378, 2006.

[46] Y. Ercan, "Akışkan gücü kontrolü teorisi," 1995.

[47] M. Barr, "Pulse width modulation," *Embedded Systems Programming*, vol. 14, no. 10, pp. 103–104, 2001.

[48] K. J. Åström and K. Furuta, "Swinging up a pendulum by energy control," *Automatica*, vol. 36, no. 2, pp. 287–295, 2000.